IEEE Access
Multidisciplinary | Rapid Review | Open Access Journal

Received January 25, 2019, accepted February 18, 2019, date of publication February 28, 2019, date of current version March 25, 2019.

Digital Object Identifier 10.1109/ACCESS.2019.2902325

Total Variation Based Joint Detection and State Estimation for Wireless Communication in Smart Grids

ANKIT KUDESHIA[1], (Student Member, IEEE), ADITYA K. JAGANNATHAM[1], (Member, IEEE), AND LAJOS HANZO[2], (Fellow, IEEE)

[1]Department of Electrical Engineering, IIT Kanpur, Kanpur 208016, India
[2]School of Electronics and Computer Science, University of Southampton, Southampton SO17 1BJ, U.K.

Corresponding author: Lajos Hanzo (lh@ecs.soton.ac.uk)

This work was supported in part by the Advanced Communication and Control for The Prevention of Blackouts (ACCEPT) Project funded by the Department of Science and Technology, Government of India. The work of L. Hanzo was supported in part by the Engineering and Physical Sciences Research Council under Project EP/Noo4558/1, Project EP/PO34284/1, and Project COALESCE, of the Royal Society's Global Challenges Research Fund Grant, and in part by the European Research Council's Advanced Fellow Grant QuantCom.

ABSTRACT A novel total variation (TV) framework is conceived for joint detection and dynamic state estimation (JDSE) for wireless transmission from the measurement devices to the control center in a smart grid. The proposed scheme employs a TV regularization based decoder in conjunction with a Kalman filter-based dynamic power system state estimator to minimize the detection error for transmission of the measurements over a fading wireless channel. A novel application of the Viterbi algorithm is proposed for TV detection of the received measurement vectors. Furthermore, the proposed JDSE scheme is also extended to a system in which each measurement is quantized to a single bit. This reduced-bandwidth-based TV-JDSE leads to a significant bandwidth efficiency improvement in the smart grid and to improved state estimation. Our simulation results provided for the standard IEEE−14 bus test system under different operating conditions demonstrate improved performance in comparison to conventional techniques and they are capable of approaching the ideal Clairvoyant Kalman filter benchmark.

INDEX TERMS Smart grids, dynamic state estimation, Kalman filter, total variation, Viterbi algorithm, wireless communication, PMU, SCADA.

I. INTRODUCTION

The increasing demand for electric power has led to severe challenges in ensuring reliable, efficient and economic operation of the existing power grid infrastructure. Conventional grids lack intelligent mechanisms for avoiding equipment failures, meeting the steep rise in demand for energy at peak hours, integration of renewable energy sources, among others, which makes the grid prone to power outages and blackouts. Therefore, smart grids [1], [2] that incorporate advanced capabilities into the conventional electrical grid for improving the reliability, safety and efficiency of power system operation, have gained significant popularity [3], [4]. A key focus of research in smart grids is the development of intelligent techniques for the prediction, prevention and correction of faults for realizing the above goals [5], [6]. This is possible through real time monitoring and control of the power system that is performed at the control center or energy management system (EMS) [7], [8] via state estimation [9]. The power system state, which provides vital information regarding its various components, is estimated via various measurements that are collected from the different components of the power system and it includes the voltage magnitude and the phasor information at the different buses. Thus, state estimation plays a central role in meeting the desired objectives of smart grid operation. These measurements are subsequently transmitted over a communication channel for processing at the control center for dynamic state estimation. Accurate state estimation based on the received measurements is of utmost importance to meet the stringent specifications of the smart grid [10]. The next subsection describes the existing research and challenges for communication in smart grids.

The associate editor coordinating the review of this manuscript and approving it for publication was Andrea M. Tonello.

A. WIRELESS COMMUNICATION FOR SMART GRID

Modern digital communication technologies, which can be readily deployed and scaled, are essential for reliable and

efficient functioning of a smart grid [11]–[13]. In this context, the papers [14]–[18] describe various communication technologies and the ensuing challenges. Conventional wireline systems, such as those based on optical fibers, power line communication [19], copper wires etc., lack the flexibility required for rapid deployment and for meeting the requirements of a rapidly expanding grid. On the other hand, wireless technologies are gaining popularity for smart grid applications due to their low infrastructure costs coupled with fast deployability, especially in difficult-to-access remote locations. However, a fundamental shortcoming of wireless communication technologies is their high error rate [20], which arises due to the severe fading nature of the wireless channel. Furthermore, electromagnetic noise arising due to the corona effect [21] and the electric discharge between the different line components in a power system [22] also degrade the quality of the wireless signal. These factors lead to erroneous detection of the measurements at the control center, in turn resulting in faulty state estimation, hence preventing reliable operation. To enhance the reliability of wireless communication, error control coding-based communication techniques have been proposed in [23] and [24]. However, these schemes impose significant overheads, and are thus unsuitable for high traffic phasor measurement unit (PMU) measurement communication. Sharma and Samantaray [25] describe a procedure for robust state estimation in smart grids that utilizes a state forecasting approach to obtain pseudo measurements during temporary disruptions of the communication link, which impose data packet losses. Thus, there is significant scope for the development of techniques that improve the accuracy of measurement detection at the receiver followed by accurate state estimation at the control center. To this end, total variation (TV) regularization has shown significantly improved performance for signal recovery in various practical applications pertaining to signal denoising [26], image/video deblurring [27], image/video recovery in wireless sensor networks [28], compressive sensing [29] etc. The proposed scheme therefore incorporates TV regularization for joint detection and dynamic state estimation (JDSE) in smart grids. This is achieved via a novel application of the Viterbi algorithm to evaluate the optimal solution of the TV regularized cost minimization problem. Furthermore, a significant drawback of the existing schemes designed for dynamic state estimation [30]–[36] in smart grids is that they employ analog measurements, which are not suited for direct transmission in digital wireless communication systems. Explicitly, the measurements have to be quantized [37] and subsequently digitally modulated prior to transmission over high speed wireless links. Therefore, we conceive practical schemes based on quantized measurements, relying on a limited number of bits, and the pertinent optimal decoder. In order to further reduce the bandwidth required, $1-$bit quantization based reduced-bandwidth (RB) schemes are developed for both PMU and conventional supervisory control and data acquisition (SCADA) measurements, thereby improving the spectral efficiency and in turn making the communication infrastructure scalable. The organization and contributions of the paper are briefly described next.

B. CONTRIBUTIONS OF THE PAPER

- Against the above background, in this paper, a novel framework is proposed for improved-accuracy state estimation in smart grids relying on the wireless transmission of measurements from the measurement devices (PMU/SCADA) to the control center. The schemes advocated consider only quantized measurements, thus making them relevant for practical implementation with digital modulation for wireless communication.
- A TV regularized cost function is developed at the receiver, which exploits the bounded temporal variation of the state vector sequence to overcome the high error rate arising due to the fading nature of the wireless channel.
- Furthermore, a novel application of the Viterbi algorithm is conceived for estimating the optimal state vector sequence as the solution to the TV regularized joint detector and Kalman filter (KF)-based dynamic state estimator [38].
- Additionally, a reduced-bandwidth scheme is developed for quantization of the analog measurements using only a single bit per measurement, which significantly reduces the bit rate required for communication in the smart grid.
- Simulation results are presented to illustrate the performance of the proposed schemes and to compare it with that of conventional schemes, under different operational conditions of the standard IEEE$-$14 bus power system.

C. ORGANIZATION OF THE PAPER

The organization of the rest of the paper is as follows. Section II presents linear and non-linear power system measurement models followed by measurement quantization and subsequent transmission over a fading wireless channel. This is followed by a brief description of the conventional maximum likelihood (ML) detector and the proposed TV regularized enhancement in Section III. The scheme for Viterbi algorithm based TV regularized joint detection and state estimation (TV-JDSE) is also detailed therein. Next, in Section IV, reduced-bandwidth schemes (RB-JDSE and TV-RB-JDSE) are presented, wherein the analog measurements are quantized to a $1-$bit message prior to transmission over the wireless channel followed by joint detection and state estimation at the receiver. Section V presents the simulation setup and the simulation results, followed by our conclusions in Section VI. Appendices in the end present our proofs for the various analytical propositions.

D. SYMBOLS AND NOTATIONS

Scalars, vectors and matrices are denoted by lower case letters (a), lower case boldface letters ($\mathbf{a}$) and upper case boldface letters ($\mathbf{A}$), respectively. $\mathbb{E}\{f\,(x)\}$ denotes the stan-

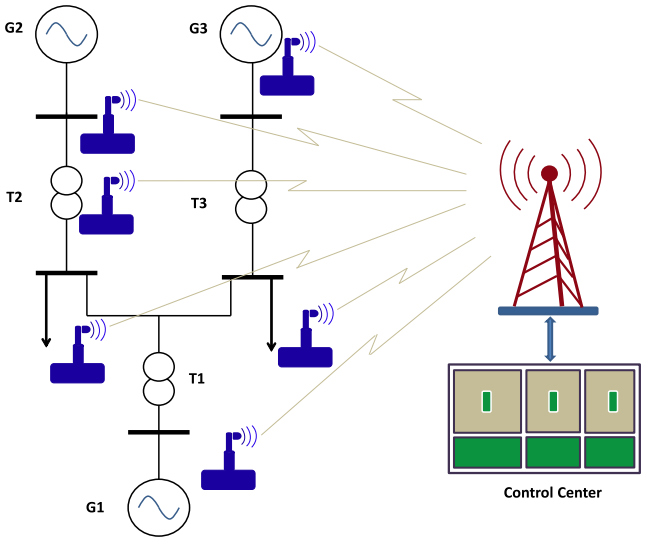

FIGURE 1. Schematic diagram of an $p-$bus power system in a smart grid with wireless communication.

dard expectation operator which returns the stochastic average of the function $f(x)$ with respect to the probability density function (PDF) of random parameter x. $\hat{\mathbf{x}}$ denotes the estimate of $\mathbf{x}$. $\mathbb{R}$, $\mathbb{C}$ denote the set of real and complex numbers, respectively. $Q[\cdot]$ denotes the tail probability function of the standard normal random variable that is defined as $Q[t] = \frac{1}{\sqrt{2\pi}} \int_t^\infty \exp\left[-\frac{u^2}{2}\right] du$. $\mathcal{N}[\boldsymbol{\mu}, \mathbf{C}]$ represents the multivariate normal distribution with mean $\boldsymbol{\mu}$ and covariance $\mathbf{C}$. diag $(\mathbf{x})$ denotes an $n \times n$ diagonal matrix with diagonal elements given by vector $\mathbf{x}$ of size $n \times 1$. $\mathbf{I}_m$ represents an identity matrix of size $m \times m$.

II. SMART GRID MEASUREMENT AND WIRELESS COMMUNICATION MODEL

Consider a $p-$bus power system in a smart grid relying on wireless communication as shown in Fig. 1. To monitor the smart grid, various measurement devices are installed for monitoring the different buses in the power system. These are either phasor measurement units (PMU) that obtain synchrophasor measurements, or conventional devices that measure the injected and transferred real and reactive powers, power flows etc. The $p-$bus power system at time instant n is fully characterized by the p voltage magnitudes $V_{i,n}$, $1 \leq i \leq p$ and the $p-1$ phasors $\delta_{i,n}$, $2 \leq i \leq p$, since the phasor corresponding to the reference bus 1 is set as $\delta_{1,n} = 0$. The quantities $V_{i,n}, \delta_{i,n}$ are termed the state variables and the corresponding state vector $\mathbf{x}_n \in \mathbb{R}^{P\times 1}$ at time instant n is defined as

$$\mathbf{x}_n = \left[V_{1,n}, V_{2,n}, \ldots, V_{p,n}, \delta_{2,n}, \delta_{3,n} \ldots \delta_{p,n}\right]^T, \quad (1)$$

where $P = 2p - 1$ and $1 \leq n \leq N$, with N denoting the total number of time instants.

Let $\mathbf{z}_n \in \mathbb{R}^{M\times 1}$ denote the corresponding measurement, where M denotes the number of measurements [39], [40] at each time instant. The measurement vector in the smart grid is obtained as per one of the models described below.

In the PMU measurement model, PMUs that measure the voltage phasors are assumed to be installed at all the buses in the power system. The measurement process for such a setup can be described by the linear model [41]

$$\mathbf{z}_n = \mathbf{x}_n + \mathbf{r}_n, \quad (2)$$

where $\mathbf{r}_n$ denotes the additive Gaussian measurement noise that has zero mean and the error covariance matrix of $\mathbb{E}\{\mathbf{r}_n \mathbf{r}_n^T\} = \mathbf{C}_r$, which is attributed to measurement uncertainties, similar to other related contributions, such as [42]–[44]. It can be seen that for the PMU model, the number of measurements obeys $M = P$. Furthermore, for the specific scenario wherein the PMUs measure the current phasors instead of the voltage phasors, the measurement model in (2) and the proposed scheme can be suitably modified for dynamic state estimation from the measurements.

By contrast, the conventional voltage magnitude measurement process is described by the SCADA measurement model as follows

$$\mathbf{z}_n = \mathbf{h}(\mathbf{x}_n) + \mathbf{r}_n, \quad (3)$$

where $\mathbf{h}(\mathbf{x}_n) \in \mathbb{R}^{M\times 1}$ is a function of the state vector $\mathbf{x}_n$. It can be observed that when the elements of the measurement vector $\mathbf{z}_n$ also include the real and reactive injection powers and the power flow of the various buses, the resultant model is a non-linear function of the state vector $\mathbf{x}_n$. Although the proposed dynamic state estimation schemes are developed for the measurement model in (3), its scope can be readily broadened to a non-linear model employing the extended or unscented Kalman filter frameworks.

One can now employ a suitable state estimator [9] for the estimation of the state vector $\mathbf{x}_n$ from the measurements. A majority of the state estimators proposed in the existing literature can be classified as being either static or dynamic in nature. However, the accuracy of static state estimation (SSE) [45]–[47] schemes is typically poor since it fails to exploit state evolution, which is an important characteristic of power systems. By contrast, dynamic state estimators (DSE) [30], which predict the variation of the state followed by estimation, are better suited for smart grids [48] and thus form the focus of this work. A pair of popular models for the time evolution of the state vector $\mathbf{x}_n$ in a power grid, frequently invoked by the existing contributions on dynamic state estimation, are briefly described below. The linear discrete-time evolution model [49] that captures the quasi steady-state behavior of the power system is

$$\mathbf{x}_{n+1} = \tilde{\mathbf{F}}_n \mathbf{x}_n + \mathbf{q}_n, \quad (4)$$

where $\tilde{\mathbf{F}}_n = \alpha_n \mathbf{I}_P$ is the state transition matrix at time-instant n, which characterizes the rate of evolution of the state vector. The vector $\mathbf{q}_n \in \mathbb{R}^{P\times 1}$ represents the model noise that is additive Gaussian with zero-mean and covariance matrix $\mathbf{C}_q$. A slightly more sophisticated dynamic model that incorporates *a priori* knowledge of the system's behavior, termed as

the linear exponential smoothing (LES) model [42], is given as follows

$$\mathbf{x}_{n+1} = \mathbf{F}_n \mathbf{x}_n + \mathbf{g}_n + \mathbf{q}_n. \tag{5}$$

The additional parameter vector $\mathbf{g}_n$ of this model depends on the behavior of the state trajectory. The matrix $\mathbf{F}_n$ and vector $\mathbf{g}_n$ are defined as

$$\mathbf{F}_n = w_1 (1 + w_2) \mathbf{I}_P, \tag{6}$$

$$\mathbf{g}_n = (1 + w_2)(1 - w_1) \hat{\mathbf{x}}_{n|n-1} - w_2 \mathbf{a}_{n-1} + (1 - w_2) \mathbf{b}_{n-1}, \tag{7}$$

where the parameters w_1 and w_2 are computed using Holt's technique [42] for online parameter estimation and typically belong to the range $0 \leq w_1, w_2 \leq 1$. Furthermore, $\hat{\mathbf{x}}_{n|n-1}, \hat{\mathbf{x}}_{n|n}$ denote the predicted and *a posteriori* estimates of the state vector at time instant n, obtained using the previous $n-1$, n observations, respectively. The vector parameters $\mathbf{a}_n \in \mathbb{R}^{P\times 1}$ and $\mathbf{b}_n \in \mathbb{R}^{P\times 1}$ are computed as

$$\mathbf{a}_n = w_1 \hat{\mathbf{x}}_{n|n} + (1 - w_1) \hat{\mathbf{x}}_{n|n-1}, \tag{8}$$

$$\mathbf{b}_n = w_2 (\mathbf{a}_n - \mathbf{a}_{n-1}) + (1 - w_2) \mathbf{b}_{n-1}. \tag{9}$$

The estimation error covariance matrices $\hat{\mathbf{M}}_{n|n-1}$ and $\hat{\mathbf{M}}_{n|n}$ of the predicted (*a priori*) and updated (*a posteriori*) estimates, respectively at time-instant n are defined as

$$\hat{\mathbf{M}}_{n|n-1} = \mathbb{E}\{\left(\hat{\mathbf{x}}_{n|n-1} - \mathbf{x}_n\right)\left(\hat{\mathbf{x}}_{n|n-1} - \mathbf{x}_n\right)^T\}, \tag{10}$$

$$\hat{\mathbf{M}}_{n|n} = \mathbb{E}\{\left(\hat{\mathbf{x}}_{n|n} - \mathbf{x}_n\right)\left(\hat{\mathbf{x}}_{n|n} - \mathbf{x}_n\right)^T\}. \tag{11}$$

The next section details the wireless model of conveying the measurement vector $\mathbf{z}_n$ from the measurement devices to the control center in the smart grid.

A. WIRELESS CHANNEL MODEL

Wireless communication facilitates the prompt transmission of the measurements from the different buses equipped with measurement devices such as SCADA systems/PMUs etc, to the control center for effective monitoring of the smart grid. Due to the digital modulation schemes such as QPSK, M-QAM etc. that are typically employed in state-of-the-art wireless systems, one cannot directly transmit the analog measurement vector $\mathbf{z}_n$ over the wireless channel. Hence, prior to transmission, each element $\mathbf{z}_n(m)$ of the measurement vector $\mathbf{z}_n$ is quantized to one of the N_q levels $\zeta_m(i) \in \zeta_m, 1 \leq i \leq N_q$ to obtain the quantized value $\check{\mathbf{z}}_n(m)$. This operation can be described as

$$\check{\mathbf{z}}_n(m) = f_q\left[\mathbf{z}_n(m)\right], \tag{12}$$

where f_q represents the quantizer. The set ζ_m is comprised of the N_q quantization levels corresponding to the mth measurements device. The vector $\check{\mathbf{z}}_n$ is comprised of the quantized measurements in $\mathbf{z}_n$. Each of the quantized measurements $\check{\mathbf{z}}_n(m)$ is then digitally modulated at the transmitter as described below. Consider a digital symbol constellation $\mathcal{S}$ with R symbols, i.e., $|\mathcal{S}| = R$, with each symbol representing $\log_2 R$ bits. For instance, popular constellations are BPSK ($R = 2$), QPSK ($R = 4$), 16−QAM ($R = 16$) etc. Since the set ζ_m is comprised of the N_q quantization levels, $N_s = \frac{\log_2 N_q}{\log_2 R}$ symbols $\boldsymbol{\xi}_n^m(1)$, $\boldsymbol{\xi}_n^m(2)$, …, $\boldsymbol{\xi}_n^m(N_s)$ are required to transmit each quantized measurement $\check{\mathbf{z}}_n(m)$, which are represented by the transmit vector $\boldsymbol{\xi}_n^m$. Thus we have $\boldsymbol{\xi}_n^m = \phi\left(\check{\mathbf{z}}_n(m)\right) \in \mathbb{S} = \prod_{i=1}^{N_s} \mathcal{S}$ where $\phi(.)$ denotes the modulation operation.

The modulated symbols are subsequently transmitted over a wireless channel. The multipath nature of the wireless channel leads to fading, which results in high bit error rate (BER) for the measurements of the smart grid communicated over the wireless channel. Thus, for reliable operation of the smart grid, we need efficient schemes for minimizing the BER of the measurements received at the control center. Let the flat-fading wireless channel corresponding to the mth measurement device at time instant n be characterized by the channel coefficient h_n^m. It can be obsedrved that this model is general and covers a fast-fading scenario in which the coefficients h_n^m are distinct for each time instant, as well as the slow-fading scenario with the corresponding coefficients h_n^m being constant for all n. The input-output model [20] of the wireless system that relates the received signal $\mathbf{y}_n^m(i) \in \mathbb{C}$ corresponding to the ith transmitted symbol $\boldsymbol{\xi}_n^m(i) \in \mathcal{S}$ is given by the following equation,

$$\mathbf{y}_n^m(i) = h_n^m \boldsymbol{\xi}_n^m(i) + \boldsymbol{\eta}_n^m(i). \tag{13}$$

Therefore, the input-output wireless transmission-reception model that relates the received signal vector $\mathbf{y}_n^m \in \mathbb{C}^{N_s}$ to the transmitted symbol vector $\boldsymbol{\xi}_n^m$ is given by

$$\mathbf{y}_n^m = \mathbf{H}_n^m \boldsymbol{\xi}_n^m + \boldsymbol{\eta}_n^m, \tag{14}$$

where the matrix $\mathbf{H}_n^m \in \mathbb{C}^{N_s \times N_s}$ for the mth measurement at time instant n is

$$\mathbf{H}_n^m = \begin{bmatrix} h_n^m & 0 & \dots & 0 \\ 0 & h_n^m & \dots & 0 \\ \vdots & \vdots & \ddots & \vdots \\ 0 & 0 & \dots & h_n^m \end{bmatrix}. \tag{15}$$

The quantity $\boldsymbol{\eta}_n^m$ denotes the additive white Gaussian noise (AWGN) vector comprising the zero-mean noise samples $\boldsymbol{\eta}_n^m(i)$ of variance σ_η^2, which is frequently used for modeling the noise at the receiver in wireless communication systems [20], [50]–[53]. The next section describes the procedure of minimizing the error in dynamic state estimation at the receiver arising due to the various imperfections such as fading, measurement and thermal noise.

III. TV-REGULARIZATION BASED JOINT DETECTION AND DYNAMIC STATE ESTIMATION (TV-JDSE)

Conventionally, the maximum likelihood (ML) detector [20] is employed to obtain the estimate $\hat{\boldsymbol{\xi}}_n^m$ of the transmitted symbol vector $\boldsymbol{\xi}_n^m$ from the received signal $\mathbf{y}_n^m$ at the receiver, as shown below

$$\hat{\boldsymbol{\xi}}_n^m = \underset{\boldsymbol{\xi}_n^m \in \mathbb{S}}{\arg\min} \|\mathbf{y}_n^m - \mathbf{H}_n^m \boldsymbol{\xi}_n^m\|_2^2. \tag{16}$$

This is subsequently employed for dynamic state estimation at the control center. However, the above conventional approach leads to a high error rate in the reconstructed measurements due to the fading nature of the wireless channel. Furthermore, a significant weakness of the above conceptually simple detector is that it does not incorporate the power system dynamics in (4) and (5) for joint detection and state estimation.

To overcome the above shortcomings, a novel total variation (TV) regularization [54] based joint detector and state estimator (JDSE) is developed below, which exploits the bounded variation (BV) property [55], [56] of the state vector time-series $\boldsymbol{\Xi}^m = \left[\boldsymbol{\xi}_1^m, \boldsymbol{\xi}_2^m \cdots \boldsymbol{\xi}_N^m\right]$, for the power system under consideration. Thus, it achieves robust dynamic state estimation from the noisy signal vectors $\mathbf{y}_n^m$ received over the fading channel for improved accuracy of measurement reconstruction. To develop the TV cost-function, consider the received signal vector over N time instants represented by the concatenated matrix $\mathbf{Y}^m = \left[\mathbf{y}_1^m, \mathbf{y}_2^m \cdots \mathbf{y}_N^m\right] \in \mathbb{C}^{N_s \times N}$. The estimated transmit vector sequence $\hat{\boldsymbol{\Xi}}^m = \left[\hat{\boldsymbol{\xi}}_1^m, \hat{\boldsymbol{\xi}}_2^m \cdots \hat{\boldsymbol{\xi}}_N^m\right] \in \mathcal{S}^{N_s \times N}$ corresponding to the time-series $\mathbf{x}_n(m), 1 \leq n \leq N$ of the mth measurement is given by the maximum *a posteriori* probability (MAP) rule [38]

$$\begin{aligned}\hat{\boldsymbol{\Xi}}^m &= \underset{\boldsymbol{\Xi}^m \in \mathcal{S}^{N_s \times N}}{\arg\max}\ P\left(\boldsymbol{\Xi}^m | \mathbf{Y}^m\right) \\ &= \underset{\boldsymbol{\Xi}^m \in \mathcal{S}^{N_s \times N}}{\arg\max}\ P\left(\mathbf{Y}^m | \boldsymbol{\Xi}^m\right) \times P\left(\boldsymbol{\Xi}^m\right) \\ &= \underset{\boldsymbol{\Xi}^m \in \mathcal{S}^{N_s \times N}}{\arg\max} \prod_{n=1}^{N} P\left(\mathbf{y}_n^m | \boldsymbol{\xi}_n^m\right) \times \prod_{n=1}^{N} P\left(\boldsymbol{\xi}_n^m\right). \end{aligned} \quad (17)$$

The probability density function (PDF) $P\left(\mathbf{y}_n^m / \boldsymbol{\xi}_n^m\right)$ follows the Gaussian distribution as determined by the input-output relationship in (14). On the other hand, the term $P\left(\boldsymbol{\xi}_n^m\right)$ represents the *a priori* distribution, which is characterized by the Gibbs measure [57] given by

$$P\left(\boldsymbol{\xi}_n^m\right) = \frac{1}{\sigma_z} e^{-U\left(\boldsymbol{\xi}_n^m\right)}. \quad (18)$$

The quantity σ_z is a suitable normalizing factor and $U\left(\boldsymbol{\xi}_n^m\right)$ is the *prior* energy functional considered to be the TV norm of the transmitted symbol vectors $\boldsymbol{\xi}_n^m$. Hence, the MAP detector above reduces to evaluation of the time-series estimate $\hat{\boldsymbol{\Xi}}^m$ that minimizes the TV regularized cost-function of

$$\hat{\boldsymbol{\Xi}}^m = \underset{\boldsymbol{\Xi}^m \in \mathcal{S}^{N_s \times N}}{\arg\min} \sum_{n=1}^{N} \left(\left\| \mathbf{y}_n^m - \mathbf{H}_n^m \boldsymbol{\xi}_n^m \right\|_2^2 + \gamma \left\| \boldsymbol{\xi}_n^m \right\|_{TV} \right). \quad (19)$$

The TV regularization exploits the bounded variation (BV) property arising from the quasi-static behaviour of the power systems under normal operating conditions [30], [58]. In essence, the TV term $\|\boldsymbol{\xi}_n^m\|_{TV}$ characterizes the temporal correlation of the state vector elements and it is mathematically defined as the integral of the absolute temporal gradient of the state vector sequence [59]. Hence, for a discrete vector sequence $\mathbf{x}_n(m)$ it can be defined in terms of the l_1 norm of the difference between the current and the previous state vectors similar to [26]–[28], as shown below

$$\left\| \boldsymbol{\xi}_n^m \right\|_{TV} = \left\| \mathbf{x}_n(m) - \mathbf{x}_{n-1}(m) \right\|_1. \quad (20)$$

The Lagrange parameter γ is the regularization parameter [57] that controls the weight assigned to the TV regularization factor vis-a-vis the observation error $\|\mathbf{y}_n^m - \mathbf{H}_n^m \boldsymbol{\xi}_n^m\|_2^2$. It is worth noting that the above MAP cost-function yields a tractable framework for the decoding of the state vector sequence $\boldsymbol{\xi}_n^m$. By contrast, other related approaches such as minimum mean squared error (MMSE) estimation etc are intractable due to the non-linearity of the quantization operation in (12) and also owing to the large dimensionality of the state space. Moreover, the linear MMSE (LMMSE) approach, which minimizes the mean squared l_2 norm of the estimation error fails to exploit the sparsity arising due to the bounded variation (BV) property. Finally, the traditional compressive sensing (CS) framework [60] is not well suited either since the diagonal channel matrix $\mathbf{H}_n^m$ is of full rank, in contrast to a CS problem, wherein the dictionary matrix comprises of an over complete basis with number of observations i.e. the dimension of $\mathbf{y}_n^m$ much smaller than that of the transmit symbol vector $\boldsymbol{\xi}_n^m$.

Direct minimization of the cost-function in (19) for detection of the sequence $\hat{\boldsymbol{\Xi}}^m$ has a potentially excessive complexity since the size of the symbol vector sequence space is of the order of $\mathcal{O}\left(\left(N_q\right)^N\right)$. This renders the problem of optimal sequence detection formidable via conventional approaches. Thus, in order to overcome this challenge, a novel Viterbi algorithm based decoder is developed below for the minimization of the TV cost function of (19) for the computation of the optimal state vector sequence estimate $\hat{\boldsymbol{\xi}}_l^m$ from the received signal time-series $\mathbf{Y}^m$.

A. VITERBI DECODER FOR TV-JDSE

The proposed Viterbi-based TV-JDSE scheme employs a trellis that has N_q states and N stages, which corresponds to the N time instants, considered as shown in Fig. 2. The ith state corresponds to the transmitted symbol vector $\boldsymbol{\nu}_i \in \mathbb{S}$ for $1 \leq i \leq N_q$, where each $\boldsymbol{\nu}_i$ represents one of the N_q quantization levels in ζ_m. The state metric $\Psi_n^m(i)$ corresponding to state i at stage n is defined as

$$\Psi_n^m(i) = \left\| \mathbf{y}_n^m - \mathbf{H}_n^m \boldsymbol{\nu}_i \right\|_2^2 \quad \forall 1 \leq i \leq N_q. \quad (21)$$

The branch metric of the state transition from the jth state at stage $(n-1)$ to the ith state at stage n in the trellis is defined as

$$\rho_n^m(i,j) = \gamma \left| \tilde{\mathbf{x}}_n^{i,j}(m) - \hat{\mathbf{x}}_{n-1}^j(m) \right|, \quad (22)$$

where the quantity $\tilde{\mathbf{x}}_n^{i,j}(m)$ represents the state vector estimate for the transition from state j at stage $n-1$ to state i at stage n corresponding to the mth element $\mathbf{x}_n(m)$ of state vector $\mathbf{x}_n$. The step-by-step procedure of determining $\tilde{\mathbf{x}}_n^{i,j}(m)$ is comprehensively summarized in Algorithm 1, along with the update equations for the Holt parameters of $\tilde{\mathbf{g}}_n^{i,j}(m)$, $\tilde{\mathbf{a}}_n^{i,j}(m)$

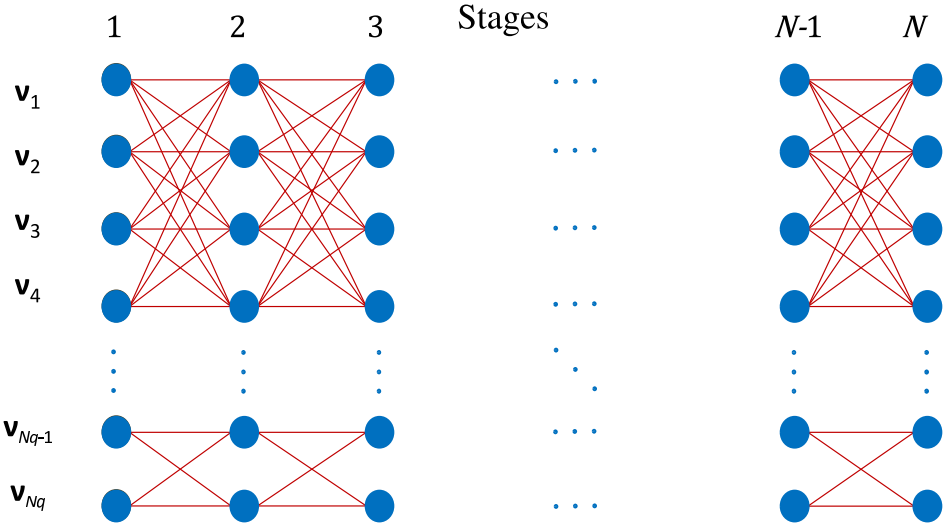

FIGURE 2. The trellis structure for the proposed TV-JDSE, RB-TV-JDSE schemes.

Algorithm 1 Viterbi Decoder Parameter Update Procedure for TV-JDSE for Transition From State j at Stage $n-1$ to State i at Stage n for mth Measurement

Input Data: i, j, m, n

Input Parameter: w_1, w_2, $\boldsymbol{\zeta}_m$, $\mathbf{g}^j_{n-1}(m)$, $\mathbf{a}^j_{n-1}(m)$, $\mathbf{b}^j_{n-1}(m)$, $\hat{\mathbf{x}}^j_{n-1}(m)$, $\hat{\mathbf{M}}^j_{n-1}(m,m)$.

Compute matrix: $\mathbf{F}_n$ using (6).

1. Prediction for state i at stage n:

$$\hat{\mathbf{x}}^{i,j}_{n|n-1}(m) = \mathbf{F}_{n-1}(m,m)\,\hat{\mathbf{x}}^j_{n-1}(m) + \mathbf{g}^j_{n-1}(m)$$

2. Update $\tilde{\mathbf{g}}^{i,j}_n(m) = (1+w_2)(1-w_1)\,\hat{\mathbf{x}}^{i,j}_{n|n-1}(m) - w_2\mathbf{a}^j_{n-1}(m) + (1-w_2)\,\mathbf{b}^j_{n-1}(m)$

3. Compute innovation for transition from state j to i at time n: $\tilde{\mathbf{z}}^{i,j}_n(m) = \boldsymbol{\zeta}_m(i) - \hat{\mathbf{x}}^{i,j}_{n|n-1}(m)$.

4. Prediction error variance

$$\hat{\mathbf{M}}^{i,j}_{n|n-1}(m,m) = \mathbf{F}^2_n(m,m)\,\hat{\mathbf{M}}^j_{n-1}(m,m) + \mathbf{C}_q(m,m)$$

5. Kalman gain $\mathbf{K}^{i,j}_n(m) = \frac{\hat{\mathbf{M}}^{i,j}_{n|n-1}(m,m)}{\hat{\mathbf{M}}^{i,j}_{n|n-1}(m,m)+\mathbf{C}_r(m,m)}$

6. Correction $\tilde{\mathbf{x}}^{i,j}_n(m) = \hat{\mathbf{x}}^{i,j}_{n|n-1}(m) + \mathbf{K}^{i,j}_n(m)\,\tilde{\mathbf{z}}^{i,j}_n(m)$

7. Estimation error variance

$$\tilde{\mathbf{M}}^{i,j}_n(m,m) = \left(1 - \mathbf{K}^{i,j}_n(m)\right)\hat{\mathbf{M}}^{i,j}_{n|n-1}(m,m)$$

8. Compute $\tilde{\mathbf{a}}^{i,j}_n(m)$ and $\tilde{\mathbf{b}}^{i,j}_n(m)$ as given by,

$$\tilde{\mathbf{a}}^{i,j}_n(m) = w_1\tilde{\mathbf{x}}^{i,j}_n(m) + (1-w_1)\,\hat{\mathbf{x}}^j_{n-1}(m)$$
$$\tilde{\mathbf{b}}^{i,j}_n(m) = w_2\left(\tilde{\mathbf{a}}^{i,j}_n(m) - \mathbf{a}^j_{n-1}(m)\right) + (1-w_2)\,\mathbf{b}^j_{n-1}(m)$$

and $\tilde{\mathbf{b}}^{i,j}_n(m)$ and the estimation error variance $\tilde{\mathbf{M}}^{i,j}_n(m,m)$ for each branch of the trellis, corresponding to the LES model of dynamic state evolution in (5).

The accumulated metric $\Phi^m_n(i)$ for each state at stage 1 is initialized as $\Phi^m_1(i) = \Psi_1(i)$. For the subsequent stages, i.e., $n \geq 2$, it is defined as

$$\Phi^m_n(i) = \Psi^m_n(i) + \min_{1\leq j\leq Ns}\{\Phi^m_{n-1}(j) + \rho^m_n(i,j)\}. \quad (23)$$

The corresponding survivor node for each state i at the subsequent stages $n \geq 2$ is decided as follows

$$\delta^m_n(i) = \arg\min_{1\leq j\leq Ns}\{\Phi^m_{n-1}(j) + \rho^m_n(i,j)\}. \quad (24)$$

Since the proposed scheme performs joint detection and state estimation, the survivor state vector estimate $\hat{\mathbf{x}}^i_n$ and the corresponding error covariance matrix $\hat{\mathbf{M}}^i(n)$ are also determined for each state i at the stage n as

$$\hat{\mathbf{x}}^i_n(m) = \tilde{\mathbf{x}}^{i,j}_n(m)\big|_{j=\delta^m_n(i)}, \quad (25)$$
$$\hat{\mathbf{M}}^i_n(m,m) = \tilde{\mathbf{M}}^{i,j}_n(m,m)\big|_{j=\delta^m_n(i)} \quad (26)$$

Holt parameters corresponding to the survivor node for each state i and each stage n of the trellis are obtained as

$$\mathbf{g}^i_n(m) = \tilde{\mathbf{g}}^{i,j}_n(m)\big|_{j=\delta^m_n(i)}, \quad (27)$$
$$\mathbf{a}^i_n(m) = \tilde{\mathbf{a}}^{i,j}_n(m)\big|_{j=\delta^m_n(i)}, \quad (28)$$
$$\mathbf{b}^i_n(m) = \tilde{\mathbf{b}}^{i,j}_n(m)\big|_{j=\delta^m_n(i)}. \quad (29)$$

After reaching the last stage of the trellis at $n = N$, the optimal TV-decoded symbol vector sequence $\hat{\boldsymbol{\Xi}}^m$ and the corresponding estimated state vector time-series $\hat{\boldsymbol{x}}_n(m)$ are determined as follows. The index $\hat{i}^m(N)$ of the symbol vector estimate at stage N is obtained by finding the specific state corresponding to the minimum accumulated metric as

$$\hat{i}^m(N) = \arg\min_{1\leq i\leq Ns}\Phi^m_N(i). \quad (30)$$

The symbol and the state vector estimates corresponding to the above state at stage N are given as $\hat{\boldsymbol{\xi}}^m_N = \boldsymbol{\nu}_{\hat{i}^m(N)}$ and $\hat{\mathbf{x}}_N(m) = \hat{\mathbf{x}}^{\hat{i}^m(N)}_N(m)$, respectively. The symbol vectors at the

previous stages $n \leq N$ are then decoded recursively from the minimum metric path indexed as

$$\hat{i}^m(n) = \delta_{n+1}^m\left(\hat{i}^m(n+1)\right), \quad n < N, \tag{31}$$

with the corresponding TV-optimal symbol and state vector estimates given by $\hat{\boldsymbol{\xi}}_n^m = \boldsymbol{\nu}_{\hat{i}^m(n)}$ and $\hat{\mathbf{x}}_n(m) = \hat{\mathbf{x}}^{\hat{i}^m(n)}(m)$, respectively. The bandwidth required for transmission of the measurements from the above devices can be seen to be proportional to the number of bits $\log_2(N_q)$ per measurement. The next section therefore presents a scheme for enhancing the bandwidth efficiency of measurement transmission in the smart grid by quantizing each measurement to a single bit followed by state estimation at the receiver.

IV. REDUCED-BANDWIDTH STATE ESTIMATION (RB-SE) FOR EFFICIENT WIRELESS COMMUNICATION IN SMART GRIDS

Again, the quantization and subsequent transmission of the raw measurements in (12) requires significant bandwidth and high data rates, which leads to substantial overheads and higher costs in the smart grid. This becomes increasingly burdensome for a large power system with a proportionally higher number of buses equipped with advanced measurement devices such as PMUs [61] due to the increased computational load for dynamic state estimation at the control center. In this context, the classical works by Steele [62], [63] which describe the linear and adaptive delta modulation techniques for the transmission of a binary coded analog signal, provide an excellent foundation for the development of bandwidth-efficient communication schemes for smart grid. Such limited bit-rate schemes have been found to be immensely useful in order to reduce the channel state information (CSI) feedback overhead from the receiver to the transmitter in modern wireless systems. Various schemes have been proposed towards this end, such as for quantized beamformer feedback in multiple transmit antenna systems [64], multi-user MIMO-OFDM systems [65], temporally correlated channels [66] and quantized covariance feedback for MIMO channels [67]. Furthermore, Grassmannian manifold-based techniques have gained significant appeal for codebook design with quantization, such as for beamforming in [68], multi-user MIMO precoding in [69]. Most recently, the work in [70] presents a comprehensive overview of codebook design, transmit precoding and signal detection schemes in mmWave massive MIMO system with low-resolution ADCs. The above works motivate the development of schemes for measurement transmission and subsequent state estimation for smart grid with a limited number of bits. However, the existing works reviewed above cannot be directly extended to wireless transmission and Kalman filter based dynamic power system state estimation where the signal is corrupted by measurement noise prior to being quantized for modulation. Therefore, to overcome this, an efficient one-bit measurement transmission scheme is proposed below based on the sign-of-innovation (SOI) framework in [71], which significantly improves the spectral efficiency, followed by the development of the corresponding reduced-bandwidth framework for TV-based state estimation in the power system. Consider the equivalent dynamic state evolution and measurement models for the mth measurement device, extracted from the overall model in (5) and (2), as shown below

$$\mathbf{x}_n(m) = \mathbf{F}_{n-1}(m,m)\mathbf{x}_{n-1}(m) + \mathbf{g}_{n-1}(m) + \mathbf{q}_{n-1}(m), \tag{32}$$

$$\mathbf{z}_n(m) = \mathbf{x}_n(m) + \mathbf{r}_n(m). \tag{33}$$

To reduce the bit-rate required for transmission, the innovation corresponding to each measurement device m at each time instant n is quantized to a single bit $\mathbf{v}_n(m) \in \{-1, +1\}$, which is determined as follows,

$$\mathbf{v}_n(m) = \operatorname{sgn}\left[\mathbf{z}_n(m) - \hat{\mathbf{z}}_{n|n-1}(m)\right] \quad \forall 1 \leq m \leq M \tag{34}$$

$$\operatorname{sgn}[x] = \begin{cases} 1, & \text{if} \quad x \geq 0 \\ -1, & \text{otherwise,} \end{cases} \tag{35}$$

where $\operatorname{sgn}[\cdot]$ denotes the standard signum function. Thus, in essence, the reduced-bandwidth scheme quantizes the measurement $\mathbf{z}_n(m)$ to a single bit with respect to the quantization threshold which is equal to the predicted value of the measurement $\hat{\mathbf{z}}_{n|n-1}(m) = \hat{\mathbf{x}}_{n|n-1}(m)$ at time instant n. The quantization process transforms the linear KF for state-estimation with conventional analog measurements described in Appendix-C into a non-linear filtering problem arising due to the non-linearity of the thresholding operation in (34). Therefore, the *a posteriori* PDF $p[\mathbf{x}(m)|\mathbf{v}_{1:n}(m)]$ is no longer given by the normal distribution, as in the conventional KF. This necessitates a more elaborate procedure for evaluation of the *a posteriori* PDF for computation of the MMSE estimate $\hat{\mathbf{x}}_{n|n}(m)$ of $\mathbf{x}_n(m)$ as shown below

$$\hat{\mathbf{x}}_{n|n}(m) = \int_{\mathbb{R}} \mathbf{x}_n(m)\, p[\mathbf{x}_n(m)|\mathbf{v}_{1:n}(m)]\, d\mathbf{x}_n(m) \tag{36}$$

The evaluation of the *a posteriori* PDF in $p[\mathbf{x}_n(m)|\mathbf{v}_{1:n}(m)]$ is carried out in a recursive fashion, similar to the procedure given in [71], as

$$\begin{aligned} &p[\mathbf{x}_n(m)|\mathbf{v}_{1:n-1}(m)] \\ &= \int_{\mathbb{R}} p[\mathbf{x}_n(m)|\mathbf{x}_{n-1}(m), \mathbf{v}_{1:n-1}(m)] \\ &\quad \times p[\mathbf{x}_{n-1}(m)|\mathbf{v}_{1:n-1}(m)]\, d\mathbf{x}_{n-1}(m) \\ &= \int_{\mathbb{R}} p[\mathbf{x}_{n-1}(m)|\mathbf{v}_{1:n-1}(m)] \\ &\quad \times \mathcal{N}\left[\mathbf{F}_n(m,m)\mathbf{x}_{n-1}(m), \mathbf{C}_q(m,m)\right] d\mathbf{x}_{n-1}(m), \end{aligned} \tag{37}$$

where the last equality arises since $p[\mathbf{x}_n(m)|\mathbf{x}_{n-1}(m), \mathbf{v}_{1:n-1}(m)]$ equals the Gaussian probability density function with mean $\mathbf{F}_n(m,m)\mathbf{x}_{n-1}(m)$ and variance $\mathbf{C}_q(m,m)$. Furthermore, it can now be seen that the *a posterior* PDF $p[\mathbf{x}_n(m)|\mathbf{v}_{1:n}(m)]$ can be determined as

$$\begin{aligned} &p[\mathbf{x}_n(m)|\mathbf{v}_{1:n}(m)] \\ &\quad = \alpha_n p[\mathbf{x}_n(m)|\mathbf{v}_{1:n-1}(m)] \end{aligned}$$

$$\times Q\left[-\mathbf{v}_n(m)\left(\frac{\mathbf{x}_n(m)-\hat{\mathbf{x}}_{n|n-1}(m)}{\mathbf{C}_r(m,m)}\right)\right], \quad (38)$$

where α_n is the normalization factor that is appropriately chosen for ensuring $\int_{\mathbb{R}} p[\mathbf{x}_n(m)|\mathbf{v}_{1:n}(m)]\,d\mathbf{x}_n(m)=1$. The procedure described above is challenging due to the numerical evaluation required for evaluating the various integrals in order to determine the MMSE estimate $\hat{\mathbf{x}}_{n|n}(m)$. This in turn leads to a high computational burden at both the encoder as well as the decoder that entails expensive hardware at both ends of the communication link. Thus, for simplifying the practical implementation of the proposed reduced-bandwidth scheme, the procedure above can be simplified by approximating the PDF $p[\mathbf{x}_n(m)|\mathbf{v}_{1:n-1}(m)]$ by the normal PDF shown below

$$p[\mathbf{x}_n(m)|\mathbf{v}_{1:n-1}(m)]=\mathcal{N}\left[\hat{\mathbf{x}}_{n|n-1}(m),\hat{\mathbf{M}}_{n|n-1}(m,m)\right]. \quad (39)$$

This leads to our low-complexity MMSE estimation algorithm detailed by the following proposition.

Proposition 1: For the power system model described in (32) and (33), the MMSE state estimate $\hat{\mathbf{x}}_n(m)$ and the corresponding *a posteriori* error variance $\hat{\mathbf{M}}_{n|n}(m,m)$, corresponding to the reduced-bandwidth transmission scheme described in (34), can be determined using the recursions below

$$\hat{\mathbf{x}}_{n|n-1}(m)=\mathbf{F}_{n-1}(m,m)\,\hat{\mathbf{x}}_{n-1|n-1}(m)+\mathbf{g}_{n-1}(m) \quad (40)$$

$$\hat{\mathbf{M}}_{n|n-1}(m,m)=\mathbf{F}_n^2(m,m)\,\hat{\mathbf{M}}_{n-1|n-1}(m,m)+\mathbf{C}_q(m,m) \quad (41)$$

$$\hat{\mathbf{x}}_{n|n}(m)=\hat{\mathbf{x}}_{n|n-1}(m)+\frac{\left(\sqrt{\frac{2}{\pi}}\right)\hat{\mathbf{M}}_{n|n-1}(m,m)\,\mathbf{v}_n(m)}{\sqrt{\mathbf{C}_r(m,m)+\hat{\mathbf{M}}_{n|n-1}(m,m)}} \quad (42)$$

$$\hat{\mathbf{M}}_{n|n}(m,m)=\hat{\mathbf{M}}_{n|n-1}(m,m)-\frac{\left(\frac{2}{\pi}\right)\hat{\mathbf{M}}^2_{n|n-1}(m,m)}{\mathbf{C}_r(m,m)+\hat{\mathbf{M}}_{n|n-1}(m,m)} \quad (43)$$

Proof 1: Given in Appendix A.

The step-by-step procedure for obtaining the single-bit measurements $\mathbf{v}_n(m)$, corresponding to the mth measurement device, is detailed in Algorithm 2. Since each measurement is quantized to a single bit, the modulated symbol vector $\boldsymbol{\xi}_n^m$ can now be replaced by a single symbol ξ_n^m per measurement. Furthermore, low complexity binary phase shift keying (BPSK) symbols of $\mathcal{S}_b=\{-1,+1\}$ can be used. Let the modulated symbol be represented as

$$\xi_n^m=\phi[\mathbf{v}_n(m)]. \quad (44)$$

Based on the wireless transmission model in (13), the corresponding received symbol y_n^m can be expressed as

$$y_n^m=h_n^m\xi_n^m+\eta_n^m. \quad (45)$$

Algorithm 2 RB Framework for 1−bit Quantization of the mth Measurement

Input Data: $\mathbf{z}_{1:n}(m)$, $\mathbf{x}_1(m)$, $\mathbf{x}_2(m)$
Input Parameter: Holt parameters w_1, w_2 and $\mathbf{C}_q$, $\mathbf{C}_r$
Initialize: $\hat{\mathbf{x}}_{1|1}(m)=\mathbf{x}_1(m)$, $\hat{\mathbf{M}}_{1|1}(m,m)=\mathbf{C}_q(m,m)$, $\mathbf{a}_1(m)=\mathbf{x}_1(m)$, $\mathbf{b}_1(m)=\mathbf{x}_2(m)-\mathbf{x}_1(m)$ and $\mathbf{g}_1(m)$ using (7).
Evaluate: $\mathbf{F}_n(m,m)$ using (6).
for `n=2 to N` **do**
1. State prediction: Evaluate $\hat{\mathbf{x}}_{n|n-1}(m)$ using (40).
2. Update the Holt parameter: $\mathbf{g}_n(m)=(1+w_2)(1-w_1)\,\hat{\mathbf{x}}_{n|n-1}(m)-w_2\mathbf{a}_n(m)+(1-w_2)\,\mathbf{b}_n(m)$
3. Prediction MSE update: $\hat{\mathbf{M}}_{n|n-1}(m,m)=\mathbf{F}^2_{n-1}(m,m)\,\hat{\mathbf{M}}_{n-1|n-1}(m,m)+\mathbf{C}_q(m,m)$
4. Set $\hat{\mathbf{z}}_{n|n-1}(m)=\hat{\mathbf{x}}_{n|n-1}(m)$.
5. Determine single bit measurement $\mathbf{v}_n(m)$ using (34).
6. Update state estimate $\hat{\mathbf{x}}_{n|n}(m)$ using (42).
7. Update estimation MSE $\hat{\mathbf{M}}_{n|n}(m,m)$ using (43).
8. Evaluate Holt parameters $\mathbf{a}_n(m)$ and $\mathbf{b}_n(m)$ using (8) and (9) respectively.

end for

Consider now the concatenated transmit vector $\boldsymbol{\xi}_n\in\mathcal{S}_b^{M\times 1}$ corresponding to all the measurement devices, defined as $\boldsymbol{\xi}_n=\left[\xi_n^1,\xi_n^2,\ldots,\xi_n^M\right]^T$. Note that $\mathcal{S}_b^{M\times 1}$ denotes the entire set of 2^M legitimate BPSK symbol vectors. The corresponding received symbol vector $\mathbf{y}_n=\left[y_n^1,y_n^2,\ldots,y_n^M\right]\in\mathbb{C}^{M\times 1}$, obtained by the concatenation of received symbols from the M measurement devices, is given by

$$\mathbf{y}_n=\mathbf{H}_n\boldsymbol{\xi}_n+\boldsymbol{\eta}_n, \quad (46)$$

where the matrix $\mathbf{H}_n\in\mathbb{C}^{M\times M}$ comprised of the channel coefficients corresponding to the wireless links in the smart grid is defined as $\mathbf{H}_n=\text{diag}\left(\left[h_n^1,h_n^2,\ldots,h_n^M\right]^T\right)$ and the AWGN noise is denoted by $\boldsymbol{\eta}_n=\left[\eta_n^1,\eta_n^2,\ldots,\eta_n^M\right]^T$. Employing the ML detector of (16), the symbol vector estimate $\hat{\boldsymbol{\xi}}_n$ is obtained as

$$\hat{\boldsymbol{\xi}}_n=\underset{\boldsymbol{\xi}_n\in\mathcal{S}_b^{M\times 1}}{\arg\min}\ \|\mathbf{y}_n-\mathbf{H}_n\boldsymbol{\xi}_n\|_2^2. \quad (47)$$

This is subsequently employed for state estimation at the control center and the corresponding procedure is succinctly described in Algorithm 3.

The above technique of state estimation using the ML-detected symbols along with the reduced-bandwidth transmission scheme of the smart grid is termed as RB-MLD-SE. It can be observed that the RB scheme offers several key advantages for practical wireless communication protocols in the smart grid. Firstly, it minimizes the bit-rate required for wireless communication since it only transmits a single bit per measurement per time instant. Furthermore, it does not require any knowledge of the quantization levels at the receiver, thus substantially simplifying the receiver design. The RB-MLD-SE technique can now be extended

Algorithm 3 RB Framework for Dynamic State Estimation

Input Data: $\mathbf{y}_{1:n}$, $\mathbf{x}_1$, $\mathbf{x}_2$
Input Parameter: w_1, w_2, $\mathbf{C}_q$, $\mathbf{C}_r$
Initialize: $\hat{\mathbf{x}}_{1|1} = \mathbf{x}_1$, $\hat{\mathbf{M}}_{1|1} = \mathbf{C}_q$, $\mathbf{a}_1 = \mathbf{x}_1$, $\mathbf{b}_1 = \mathbf{x}_2 - \mathbf{x}_1$ and $\mathbf{g}_1$ using (7).
Evaluate $\mathbf{F}_n$ using (6).
for n=2 to N **do**
1. State prediction: $\hat{\mathbf{x}}_{n|n-1} = \mathbf{F}_{n-1}\hat{\mathbf{x}}_{n-1|n-1} + \mathbf{g}_{n-1}$
2. Update $\mathbf{g}_n$ using (7).
3. Prediction MSE update:

$$\hat{\mathbf{M}}_{n|n-1} = \mathbf{F}_{n-1}\hat{\mathbf{M}}_{n-1|n-1}\mathbf{F}_{n-1}^T + \mathbf{C}_q$$

for m=1 to M **do**
a. Decode the single bit measurement $\hat{\mathbf{v}}_n(m) = \phi^{-1}\left(\hat{\boldsymbol{\xi}}_n(m)\right)$
b. Determine the Kalman gain $\mathbf{k}_n(m)$ and error variance $\hat{\mathbf{M}}_{n|n}(m,m)$ employing (55) and (43) respectively.
c. Estimate state $\hat{\mathbf{x}}_{n|n}(m) = \hat{\mathbf{x}}_{n|n-1}(m) + \mathbf{k}_n(m)\,\hat{\mathbf{v}}_n(m)$
end for
4. Evaluate Holt parameters $\mathbf{a}_n$ and $\mathbf{b}_n$ using (8) and (9) respectively.
end for

to leverage our TV-framework for joint detection and state estimation as described next.

A. REDUCED-BANDWIDTH TOTAL VARIATION REGULARIZATION BASED-JDSE (RB-TV-JDSE)

Similar to the TV-JDSE procedure described in Section III, TV regularization can now be readily incorporated into our RB-MLD-SE detection as shown below, and the resultant detector is termed as RB-TV-JDSE. Following a procedure similar to the one described in (19) for the MAP rule, the pertinent detector for the transmit symbol vector sequence $\boldsymbol{\Xi} = \left[\boldsymbol{\xi}_1, \boldsymbol{\xi}_2, \ldots, \boldsymbol{\xi}_N\right] \in \mathcal{S}_b^{M\times N}$ is given as

$$\hat{\boldsymbol{\Xi}} = \underset{\boldsymbol{\Xi}\in\mathcal{S}_b^{M\times N}}{\arg\min} \sum_{n=1}^{N}\left(\|\mathbf{y}_n - \mathbf{H}_n\boldsymbol{\xi}_n\|_2^2 + \gamma\,\|\boldsymbol{\xi}_n\|_{TV}\right), \quad (48)$$

where the TV regularization factor is $\|\boldsymbol{\xi}_n\|_{TV} = \|\mathbf{x}_n - \mathbf{x}_{n-1}\|_1$. It can now be seen that the above cost function is similar to the one obtained in (19), after dropping the subscript m. Hence, the Viterbi decoder can once again be employed for joint detection and state estimation. The total number of states in the pertinent trellis is $N_q = 2^M$ with the number of stages being N, where each state denoted by $\boldsymbol{v}_i$ corresponds to one of the 2^M possible combinations of the single-bit measurements transmitted by the measurement devices in the smart grid. The corresponding procedure of computing the various quantities $\tilde{\mathbf{x}}_n^{i,j}$, $\tilde{\mathbf{M}}_n^{i,j}$ together with the Holt parameters $\tilde{\mathbf{g}}_n^{i,j}$, $\tilde{\mathbf{a}}_n^{i,j}$ and $\tilde{\mathbf{b}}_n^{i,j}$ for the transitions from state j at stage $n-1$ to state i at stage n in the trellis is comprehensively detailed in Algorithm 4. The optimal detected symbol vector sequence $\hat{\boldsymbol{\Xi}}$ and the estimate of the state vector time series $\hat{\mathbf{X}} = \left[\hat{\mathbf{x}}_1, \hat{\mathbf{x}}_2, \ldots, \hat{\mathbf{x}}_N\right]$ can now be obtained via minimization of the above cost function using a procedure similar to the one described in Section-III.

Algorithm 4 Viterbi Decoder Parameter Update Procedure for RB-TV-JDSE for Transition From State j at Stage $n-1$ to State i at Stage n

Input Data: i, j, n
Input Parameter: w_1, w_2, $\mathbf{C}_q$, $\mathbf{C}_r$, $\boldsymbol{v}_i$, $\mathbf{g}_{n-1}^j$, $\mathbf{a}_{n-1}^j$, $\mathbf{b}_{n-1}^j$, $\hat{\mathbf{x}}_{n-1}^j$, $\hat{\mathbf{M}}_{n-1}^j$.
Compute matrix: $\mathbf{F}_n$ using (6).
1. State prediction at state i: $\hat{\mathbf{x}}_{n|n-1}^{i,j} = \mathbf{F}_{n-1}\hat{\mathbf{x}}_{n-1}^j + \mathbf{g}_{n-1}^j$
2. Update $\tilde{\mathbf{g}}_n^{i,j} = (1+w_2)(1-w_1)\,\hat{\mathbf{x}}_{n|n-1}^{i,j} - w_2\mathbf{a}_{n-1}^j + (1-w_2)\,\mathbf{b}_{n-1}^j$
3. Update prediction error covariance matrix:

$$\hat{\mathbf{M}}_{n|n-1}^{i,j} = \mathbf{F}_n\hat{\mathbf{M}}_{n-1}^j\mathbf{F}_n^T + \mathbf{C}_q$$

for m=1 to M **do**
a. Set sign-of-innovation bit $\mathbf{v}_n^i(m) = \phi^{-1}(\boldsymbol{v}_i(m))$
b. Evaluate Kalman gain $\mathbf{k}_n^{i,j}(m) = \frac{\left(\sqrt{\frac{2}{\pi}}\right)\hat{\mathbf{M}}_{n|n-1}^{i,j}(m,m)}{\sqrt{\mathbf{C}_r(m,m)+\hat{\mathbf{M}}_{n|n-1}^{i,j}(m,m)}}$
c. Update state estimate $\tilde{\mathbf{x}}_n^{i,j}(m) = \hat{\mathbf{x}}_{n|n-1}^{i,j}(m) + \mathbf{k}_n^{i,j}(m)\,\mathbf{v}_n^i(m)$.
end for
7. Update estimation error covariance $\tilde{\mathbf{M}}_n^{i,j}$ using (43).
8. Evaluate $\tilde{\mathbf{a}}_n^{i,j}$ and $\tilde{\mathbf{b}}_n^{i,j}$ as

$$\tilde{\mathbf{a}}_n^{i,j} = w_1\tilde{\mathbf{x}}_n^{i,j} + (1-w_1)\,\hat{\mathbf{x}}_{n|n-1}^{i,j}$$
$$\tilde{\mathbf{b}}_n^{i,j} = w_2\left(\tilde{\mathbf{a}}_n^{i,j} - \mathbf{a}_{n-1}^j\right) + (1-w_2)\,\mathbf{b}_{n-1}^j$$

V. SIMULATION RESULTS AND DISCUSSIONS

A. SIMULATION SETUP

Our simulation results are presented for the standard IEEE−14 bus ($p = 14$) power system [72] to illustrate the performance of the proposed schemes for wireless measurement transmission, detection and state estimation in the smart grid. The four different scenarios detailed below are considered for comprehensively illustrating the performance of the proposed TV-JDSE, RB-MLD-SE and RB-TV-JDSE techniques.

1) CASE-I: SMART GRID WITH PMU MEASUREMENT DEVICES UNDER NORMAL OPERATING CONDITIONS

Under normal operating conditions the power system exhibits a quasi-static behavior. Furthermore, the PMUs [73] typically collect the measurements from the grid at a very high temporal resolution of approximately 30 to 60 measurements per second. Hence, for the simulations characterizing this scenario, the PMU measurements are generated as follows. Similar to [74], the load flow is executed repeatedly for vari-

ous loading conditions with random variations in the loads at time instants $n = 1, 2, \ldots, N$ with $N = 100$. The maximum and the minimum limits on the overall load variations are set to $+25\%$ and -25% of their baseline values. The loads change gradually at each time-step due to the quasi-static behavior and the limit on load variation in a single time-step is set to $\pm 5\%$ of the previous load value. This scenario ideally captures the behavior of the smart grid and the performance of the proposed techniques for wireless transmission of the measurements under normal conditions.

2) CASE-II: MART GRID WITH SCADA MEASUREMENT DEVICES UNDER NORMAL OPERATING CONDITIONS

SCADA devices provide lower resolution measurements at a much lower frequency then PMU devices, typically of the order of one measurement per few seconds interval [75]. Thus the temporal resolution of measurement collection is much lower than in Case-I above. The generator and load profiles for this scenario have been obtained from the real time operational data of the UK's national power grid [76], thus demonstrating the performance of the proposed techniques based on practical grid data. Similar to Case-I, the corresponding voltage magnitude and phasor profiles are now obtained by repeatedly running the static load flow analysis for $N = 100$ time stamps for the generator and load power profiles considered above. Thus, this scenario demonstrates the applicability of the proposed techniques also for SCADA measurements, in addition to the PMU measurements considered in Case-I, thus illustrating the versatility of the proposed wireless communication framework.

3) CASE-III: SMART GRID WITH PMU MEASUREMENT DEVICES UNDER SUDDEN LOAD CHANGES

Typically, power grids also experience outages, thus deviating from their normal operating conditions. In such conditions, in order to prevent deviation of the power line frequency from its nominal value (e.g. 50Hz for UK/India grids), the imbalance between load and generation is corrected through a sudden outage at a PQ-bus for a short duration. To model this effect, in the above setting of the PMU measurements in Case-I, a PQ-bus in the power system is suddenly disconnected by setting its load power to zero during the time interval $45 \leq n \leq 55$ followed by carrying out the load flow analysis for $N = 100$ time instants. This results in a sudden change in the voltage magnitude and phasors, which corresponds to the transition from normal load to no-load [77] and back to normal load condition of the smart grid. This setup thoroughly examines the impact of outages, which although infrequent, may significantly affect the performance of the smart grid and in turn of the proposed techniques.

4) CASE-IV: SMART GRID WITH PMU DEVICES UNDER A SUDDEN LOAD DROP

This case arises, when there is a sudden load drop and the system transitions from an overloaded to no load condition. This occurs when the circuit breakers automatically disconnect a particular bus in the system due to overloading. To model this scenario, the load power at bus-4 is changed from 2.5 times of its base value to zero in the time interval $1 \leq n \leq 50$ and the load flow is executed by varying the other loads randomly in the range of $\pm 10\%$ of their base value in a single time-step for the time instants $1 \leq n \leq 100$. In this scenario, the variation in the voltage magnitude and phase is significantly higher in comparison to the other scenarios considered in Cases I, II, III for the smart grid and hence tests the robustness of the proposed methods.

The linear measurement model described in (2) is considered for the PMU voltage magnitude, phasor and SCADA voltage magnitude measurements in the above cases. To simulate real time PMU measurements, both the voltage magnitude and the phasor measurements are assumed to be corrupted by measurement uncertainties of 0.02% and $0.01°$, respectively [78], [79]. For conventional SCADA measurements, measurement uncertainties of 1% [80] are considered for the voltage magnitudes. The values of the other parameters in the power system are set as follows. The number of measurements i.e. the size of the state vector is $M = P = 27$, and the Holt parameters are set to $w_1 = 0.9$ and $w_2 = 0.5$ as proposed in [25], [36], and [74]. Similarly to [36] and [81], considering the initial states at time-instants $n = 0, 1$ to be known accurately, the diagonal elements of the prediction error covariance matrix $\mathbf{C}_q$ are set to 10^{-6}. Furthermore, the elements of the measurement noise vector $\mathbf{r}_n$ are considered to be i.i.d Gaussian distributed with zero mean and variance σ_r^2. Thus, the noise covariance matrix is $\mathbf{C}_r = \sigma_r^2 \mathbf{I}$. The various benchmarks described below are used for comparing the performance of the proposed practical schemes. The first one is the ideal clairvoyant KF state estimator, which assumes the availability of infinite bandwidth for the transmission of the analog measurements $\mathbf{z}_n$ together with error-free reception over the wireless channel. The procedure for this is summarized in Algorithm 5 of Appendix C. The second benchmark used purely for the purpose of comparison pertains to reduced-bandwidth transmission relying on ideal error-free reception of the measurement bits, $\hat{\mathbf{v}}_n = \mathbf{v}_n$, followed by the state estimation at the control center using Algorithm 3. This is termed as Ideal RB-SE. The Rayleigh fading wireless channel coefficients are generated as $h_n = \sqrt{\frac{1}{2}}\,(h_R + j h_I)$ where h_R and h_I, are i.i.d. Gaussian random variables distributed as $\mathcal{N}\left[0, \sqrt{\frac{1}{2}}\right]$. As seen from the model above, the average power of the channel coefficients is fixed as unity i.e. $\mathbb{E}\{|h_k|^2\} = 1$. The covariance of the zero mean AWGN $\boldsymbol{\eta}_n^m$ at the receiver is set to $\mathbf{C}_\eta = \sigma_\eta^2 \mathbf{I}_b$ where $\sigma_\eta^2 = \frac{1}{\mathrm{SNR}}$ and SNR is the signal to noise ratio at the receiver. The standard mean absolute estimation error (MAEE) [36] metric is considered for characterizing the performance of state estimation in various schemes, which is defined corresponding to the mth measurement as

$$MAEE\,(m) = \frac{1}{N} \sum_{n=1}^{N} \left| \mathbf{x}_n\,(m) - \hat{\mathbf{x}}_n\,(m) \right|. \tag{49}$$

TABLE 1. Average MAEE performance for the proposed TV-JDSE, RB-TV-JDSE schemes applied on the test data set for bus 4 and 7 measurements, for cases I, II, III, IV in the standard IEEE-14 bus system.

SNR		10 dB		15 dB		20 dB	
Bus	N_q	MLD-SE	TV-JDSE	MLD-SE	TV-JDSE	MLD-SE	TV-JDSE
V_4-Case-I (in p.u.)	16	2.89×10^{-4}	1.48×10^{-4}	1.90×10^{-4}	1.42×10^{-4}	1.54×10^{-4}	1.39×10^{-4}
	64	2.41×10^{-4}	1.01×10^{-4}	1.41×10^{-4}	0.94×10^{-4}	1.05×10^{-4}	0.89×10^{-4}
	2 (RB)	0.63×10^{-2}	0.27×10^{-2}	0.33×10^{-2}	0.13×10^{-2}	0.11×10^{-2}	0.06×10^{-2}
δ_7-Case-I (in degrees)	16	0.1614	0.0849	0.1079	0.0798	0.0867	0.0771
	64	0.1096	0.0317	0.0464	0.0243	0.0291	0.0222
	2 (RB)	2.57	0.88	1.41	0.49	0.74	0.31
V_4-Case-II (in p.u.)	16	4.21×10^{-4}	3.82×10^{-4}	3.75×10^{-4}	3.46×10^{-4}	3.50×10^{-4}	3.36×10^{-4}
	64	4.03×10^{-4}	3.43×10^{-4}	3.56×10^{-4}	3.13×10^{-4}	3.16×10^{-4}	2.96×10^{-4}
	2 (RB)	6.78×10^{-4}	3.11×10^{-4}	2.84×10^{-4}	1.51×10^{-4}	1.88×10^{-4}	0.91×10^{-4}
V_4-Case-III (in p.u.)	16	3.94×10^{-4}	1.87×10^{-4}	2.52×10^{-4}	1.76×10^{-4}	2.04×10^{-4}	1.63×10^{-4}
	64	3.21×10^{-4}	1.23×10^{-4}	1.81×10^{-4}	1.04×10^{-4}	1.18×10^{-4}	0.99×10^{-4}
	2 (RB)	2.23×10^{-2}	0.34×10^{-2}	0.98×10^{-2}	0.18×10^{-2}	0.37×10^{-2}	0.096×10^{-2}
V_4-Case-IV (in p.u.)	16	7.01×10^{-2}	2.79×10^{-2}	3.85×10^{-2}	2.57×10^{-2}	2.87×10^{-2}	2.36×10^{-2}
	64	6.12×10^{-2}	1.38×10^{-2}	2.78×10^{-2}	0.97×10^{-2}	1.49×10^{-2}	0.89×10^{-2}
	2 (RB)	5.75×10^{-1}	3.72×10^{-1}	3.07×10^{-1}	2.04×10^{-1}	1.69×10^{-1}	1.23×10^{-1}

B. RESULTS AND DISCUSSIONS

1) OPTIMAL VALUE OF THE TV REGULARIZATION PARAMETER γ

The optimal value of the TV regularization parameter γ in the TV cost function described in (19) in Section III for TV-JDSE is found as follows. The average MAEE is computed over 1000 Monte Carlo simulations of the power system under consideration (IEEE−14 bus) for γ in the range of $[1, 10^6]$. The resultant MAEE values are shown in Fig. 3, where it can be observed that the optimal value of γ that minimizes the average MAEE belongs to the range [500, 5000]. Thus, rather than arbitrarily setting γ, the value of γ chosen above is guaranteed to yield the best system performance.

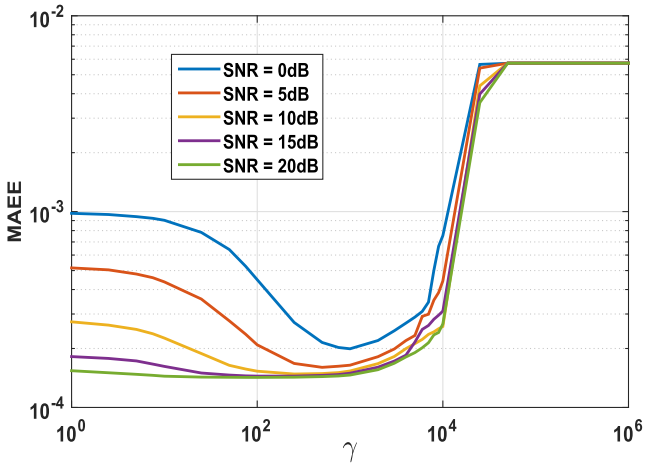

FIGURE 3. Determination of the optimal value of Lagrange parameter γ using lowest average MAEE criterion for the proposed TV-JDSE scheme for $N_q = 16$ for PMU measurements for different channel SNRs.

2) PERFORMANCE COMPARISON OF PROPOSED TV-JDSE VERSUS CONVENTIONAL MLD-SE

Results are now presented for comparing the MAEE performance of the proposed TV-JDSE to that of the conventional MLD-SE. Table-1 shows the average MAEE performance of the proposed TV-JDSE scheme for 1000 Monte Carlo simulations of the voltage magnitude and phasor measurements in the IEEE-14 bus system for Cases I, II, III and IV described above.

The voltage magnitude estimate for bus−4 and phase angle estimates for bus−7 corresponding to a normal operation scenario, such as Case-I are plotted in Fig. 4 and Fig. 5, respectively. It can be seen from Table-1, Fig. 4 and Fig. 5 that the MAEE of the TV-JDSE scheme is significantly lower than that of the conventional MLD-SE. For instance, the proposed TV-JDSE technique conceived for wireless measurement transmission leads to a reduction of more than 50% in the MAEE in comparison to the MLD-SE estimate of the bus−4 voltage magnitude for $N_q = 64$, thus illustrating the substantial improvement in performance. Similar performance improvements can be seen for $N_q = 16$ and also for various SNR values equal to 10, 15 and 20dB. Similarly, Fig. 6 and 7 plot the voltage magnitude estimate for bus−4 corresponding to the scenario of Case-III associated with sudden load changes and Case-IV with a load drop from over-loading to no-load condition. Once again,

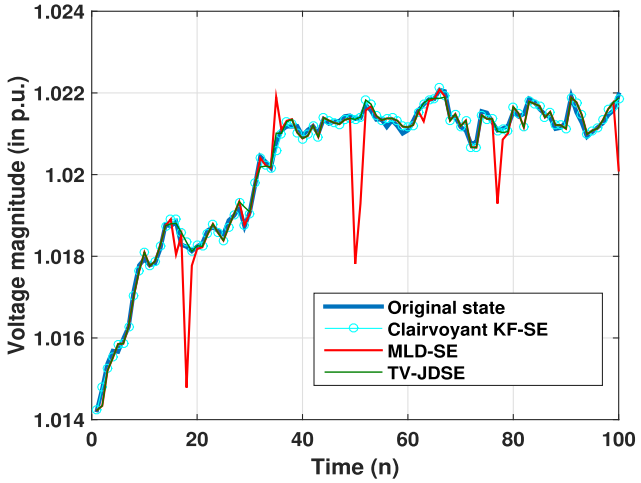

FIGURE 4. Voltage magnitude dynamic estimation using the proposed TV-JDSE scheme for bus-4 PMU measurements at SNR = 10dB and $N_q = 256$.

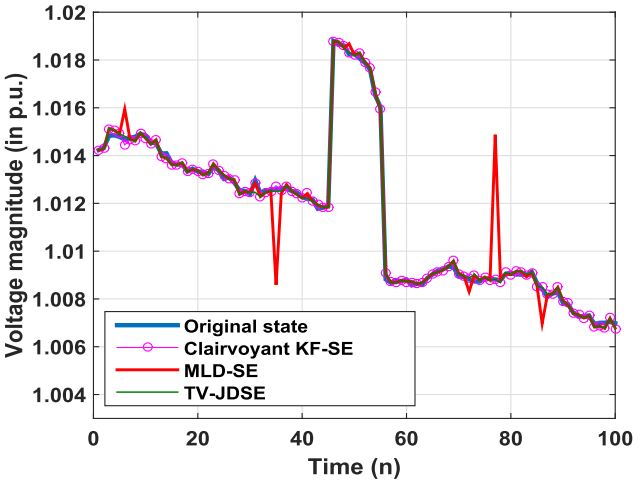

FIGURE 6. Dynamic estimation of the voltage magnitudes of bus-4 PMU measurements for the scenario in case-III using the TV-JDSE scheme at SNR = 10dB and $N_q = 256$.

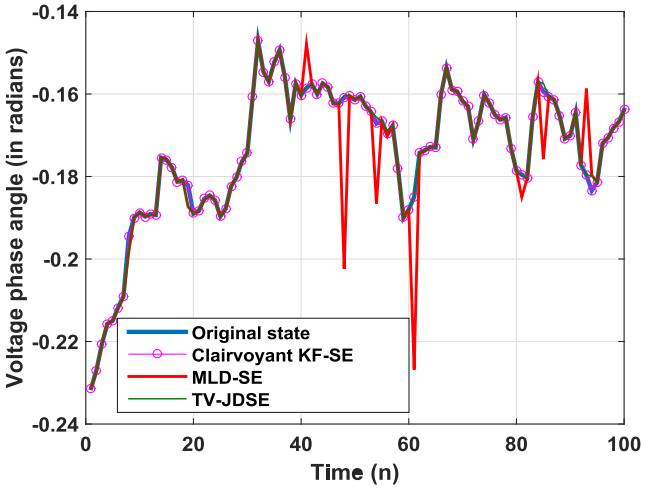

FIGURE 5. Voltage phase angle dynamic estimation for PMU measurements at bus-7 using the TV-JDSE scheme at SNR = 10dB and $N_q = 256$.

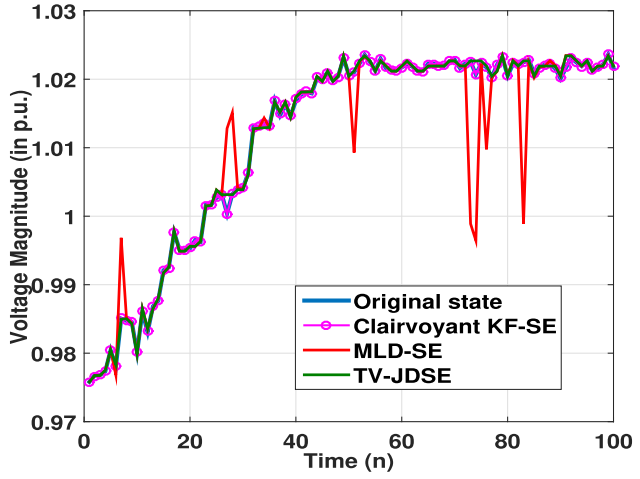

FIGURE 7. Dynamic estimation of the voltage magnitudes of bus-4 PMU measurements for the scenario in case-IV using the TV-JDSE scheme at SNR = 10dB and $N_q = 256$.

as it can be verified from Table-1, TV-JDSE leads to a 60% and 75% reduction in the MAEE over MLD-SE for $N_q = 64$ corresponding to Cases III, IV respectively at SNR = 10dB. Furthermore, the robustness of the proposed techniques manifests itself in terms of their ability to accurately track the bus voltage magnitude variations under such adverse conditions.

3) PERFORMANCE COMPARISON OF THE EFFICIENT REDUCED-BANDWIDTH (RB) SCHEMES

To characterize the performance of the proposed bandwidth efficient transmission schemes, the estimated voltage magnitude for bus-4 corresponding to the RB-TV-JDSE technique is plotted in Fig. 8 for Case-I, where it is observed that this is better suited for tracking the variations in the voltage magnitude than the conventional RB-MLD-SE. The corresponding MAEE performance averaged over 1000 Monte-Carlo simulations across the SNR range of $[0, 30]\,dB$ is shown in Fig. 9 from which it can be seen that RB-TV-JDSE yields about 50% reduction in MAEE at SNR = 10dB, as also confirmed by the values in Table-1. As the SNR is increasing, the performance of both techniques can be seen to coincide with that of the ideal RB-SE benchmark having no bit-errors. Furthermore, the average MAEE can be seen to decrease upon increasing the number of quantization levels, finally approaching the Clairvoyant KF benchmark having $N_q = 256$ levels for SNR $\geq$ 20dB. Additionally, to provide further insights, the performance of TV-JDSE and MLD-SE recorded for $N_q = 4, 16, 64, 256$ quantization levels is also shown in Fig. 9. The average MAEE can be seen to decrease upon increasing the number of quantization levels, as is naturally expected, closely approaching the Clairvoyant KF benchmark for $N_q = 256$ levels for SNR $\geq$ 20. Thus, although the RB scheme has a slightly higher MAEE, it is well suited for practical scenarios, since it only requires the transmission of

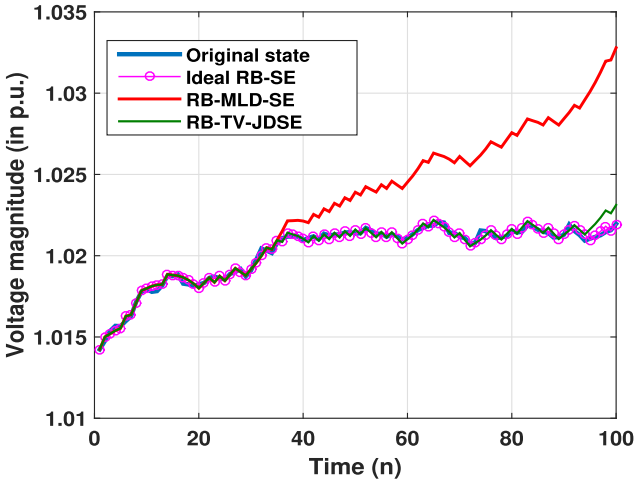

FIGURE 8. Voltage magnitude dynamic estimation using RB-TV-JDSE scheme for PMU measurements at bus-4 with SNR = 10dB.

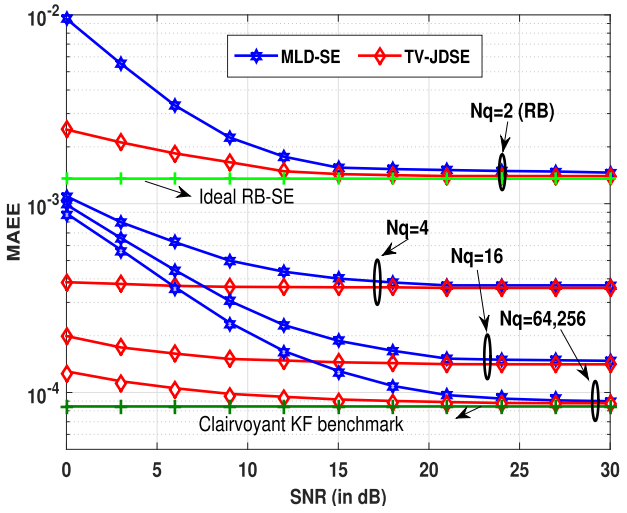

FIGURE 9. Average MAEE performance of the proposed RB-TV-JDSE and TV-JDSE schemes for $N_q = \{4, 16, 64, 256\}$ with respect to the channel SNRs for PMU measurements.

a single measurement bit. Furthermore, it can be observed that similar to the single-bit quantized MIMO aided wireless communication systems [82], [83], the proposed single-bit measurement based RB-MLD-SE and RB-TV-JDSE schemes also exhibit a flat MAEE performance at higher SNR values (typically in the range 20dB to 30dB).

4) IMPACT OF MEASUREMENT NOISE ON PERFORMANCE

Fig. 10 compares the average MAEE of the proposed TV-JDSE to that of the conventional scheme for different levels of measurement noise characterized by the variance σ_r in the range of $\left[10^{-5}, 10^{-1}\right]$ at SNR $=$ 10dB. Similar to the trends observed in the previous figures, the average MAEE of the proposed TV-JDSE is lower than that of the conventional MLD-SE for state reconstruction at different levels of the measurement noise. For instance for noise levels at $\sigma_r = 10^{-3}$ TV-JDSE yields approximately 35% reduction

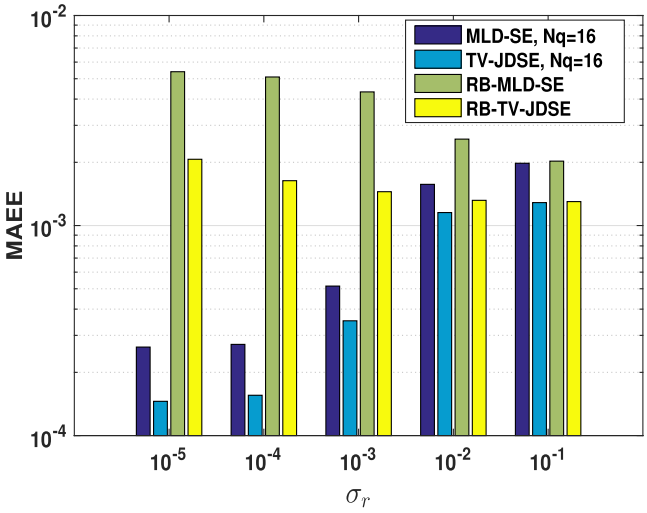

FIGURE 10. Average MAEE performance of the proposed TV-JDSE, RB-TV-JDSE schemes for bus−4 measurements at SNR = 10dB and $N_q = 16$ with respect to the measurement noise levels $\sigma_r \in \left[10^{-5}, 10^{-1}\right]$.

in MAEE in comparison to MLD-SE at $N_q = 16$, while RB-TV-JDSE yields a 60% reduction in MAEE in comparison to its RB-MLD-SE counterpart. Another interesting observation is that the RB-TV-JDSE reconstruction tends to yield a performance similar to the TV-JDSE scheme for $N_q = 16$ at higher levels of measurement noise. This is due to the fact that as $\sigma_r \to \infty$, the *a posteriori* PDF $p\left[\mathbf{x}_n(m) \,|\mathbf{v}_{1:n}(m)\right]$ converges to a normal distribution. Hence, the accuracy of the approximation in (39) improves upon increasing the value of σ_r, leading to the performance of RB-TV-JDSE becoming similar to that of TV-JDSE as $\sigma_r \to \infty$.

It can be observed from the above results that the TV-JDSE proposed for wireless measurement transmission is a better choice for state estimation in a smart grid due to the improved performance resulting from exploiting the bounded variation (BV) property [26] of the state vector sequence. Furthermore, the proposed scheme is also practical, since it is based on digital modulation schemes such as QPSK, using a finite number of quantization levels N_q. Moreover, the RB-TV-JDSE scheme that uses only a single bit per measurement is highly practical due to its extremely low bandwidth requirement, which makes it ideally suited for smart grids. These techniques are capable of significantly improving the cost-efficiency and deployability of wireless communication systems for the smart grid. Finally, the framework presented employs a simplistic encoder that does not increase the complexity of the measurement devices, which makes it even more attractive for employment in smart grids of the future.

VI. CONCLUSION

A novel TV regularization based joint measurement detector and dynamic state estimator has been proposed for robust state estimation from the measurements transmitted over a wireless channel in a smart grid. The framework developed intelligently combines the KF for dynamic state estimation in power systems with the TV detector that exploits the bounded

variation property of the state variables. The proposed scheme outperforms the conventional ML detection that leads to significant errors due to the fading nature of the wireless channel. Furthermore, a spectrally efficient TV-RB-JDSE scheme that uses single bit measurements has also been developed for dynamic state estimation, which is ideally suited for practical deployment due to its low bandwidth overhead coupled with its improved estimation accuracy. Our simulation results demonstrated the enhanced accuracy of dynamic state estimation using the proposed schemes for wireless transmission of power grid measurements over a fading wireless channel.

APPENDIX A
PROOF OF PROPOSITION 1

The predictors in (40) and (41) follow from the observation model given in (5) and (10). The MMSE estimate $\hat{\mathbf{x}}_{n|n}(m)$ in (55) is obtained by evaluating the expected value of the quantity $\mathbf{x}_n(m)$ over its *a posteriori* PDF $p[\mathbf{x}_n(m)|\mathbf{v}_{1:n}(m)]$ i.e.

$$\hat{\mathbf{x}}_{n|n}(m) = \int_{\mathbb{R}} \mathbf{x}_n(m)\, p[\mathbf{x}_n(m)|\mathbf{v}_{1:n}(m)]\, d\mathbf{x}_n(m) \quad (50)$$

The *a posteriori* PDF $p[\mathbf{x}_n(m)|\mathbf{v}_{1:n}(m)]$ follows applying the Bayes' rule as

$$\begin{aligned} &p[\mathbf{x}_n(m)|\mathbf{v}_{1:n}(m)] \\ &= p[\mathbf{x}_n(m)|\mathbf{v}_{1:n-1}(m), \mathbf{v}_n(m)] \\ &= \frac{p[\mathbf{v}_n(m)|\mathbf{x}_n(m), \mathbf{v}_{1:n-1}(m)] \times p[\mathbf{x}_n(m), \mathbf{v}_{1:n-1}(m)]}{p[\mathbf{v}_n(m)|\mathbf{v}_{1:n-1}(m)]} \end{aligned} \quad (51)$$

The various quantities above can be evaluated as described next. The PDF $p[\mathbf{v}_n(m)|\mathbf{x}_n(m), \mathbf{v}_{1:n-1}(m)]$ can be determined as

$$\begin{aligned} &p[\mathbf{v}_n(m)|\mathbf{x}_n(m), \mathbf{v}_{1:n-1}(m)] \\ &\quad = Pr\{\mathbf{v}_n(m) = \pm 1|\mathbf{x}_n(m), \mathbf{v}_{1:n-1}(m)\} \\ &\quad = Pr\{\mathbf{z}_n(m) \lessgtr \hat{\mathbf{z}}_{n|n-1}(m)|\mathbf{x}_n(m)\} \\ &\quad = Pr\{\mathbf{r}_n(m) \lessgtr \left(\hat{\mathbf{x}}_{n|n-1}(m) - \mathbf{x}_n(m)\right)|\mathbf{x}_n(m)\} \\ &\quad = Q\left[\mathbf{v}_n(m)\frac{\hat{\mathbf{x}}_{n|n-1}(m) - \mathbf{x}_n(m)}{\mathbf{C}_r(m,m)}\right]. \end{aligned} \quad (52)$$

The PDF $p[\mathbf{x}_n(m), \mathbf{v}_{1:n-1}(m)]$ is approximated as $\mathcal{N}\left[\hat{\mathbf{x}}_{n|n-1}(m), \hat{\mathbf{M}}_{n|n-1}(m,m)\right]$ as justified in (39). The conditional probability $p[\mathbf{v}_n(m) = \pm|\mathbf{v}_{1:n-1}(m)]$ can now be obtained as

$$P[\mathbf{v}_n(m)|\mathbf{v}_{1:n-1}(m)] = Pr\{\mathbf{z}_n(m) \lessgtr \hat{\mathbf{z}}_{n|n-1}(m)\} = \frac{1}{2} \quad (53)$$

The above result follows from the fact that the probability of the normal random variable $\mathbf{x}_n(m)$ leaving a value either greater or lesser than its mean value $\hat{\mathbf{x}}_{n|n-1}(m)$ equals half, together with the property that $\mathbf{z}_n(m)$ is a linear transformation of $\mathbf{x}_n(m)$ as given in (3). Upon substituting the probabilities and PDFs above in the integral of (36) to evaluate the MMSE estimate, the expression reduces to

$$\begin{aligned} \hat{\mathbf{x}}_{n|n}(m) = 2\int_{\mathbb{R}} \mathbf{x}_n(m)\, \mathcal{N}\left[\hat{\mathbf{x}}_{n|n-1}(m), \hat{\mathbf{M}}_{n|n-1}(m,m)\right] \\ \times\, Q\left[\mathbf{v}_n(m)\frac{\left(\hat{\mathbf{x}}_{n|n-1}(m) - \mathbf{x}_n(m)\right)}{\mathbf{C}_r(m,m)}\right] d\mathbf{x}_n(m). \end{aligned} \quad (54)$$

The integral in (54) can be further simplified using the procedure detailed in Appendix B, leading to the results given in (42). The Kalman gain $\mathbf{k}_n(m)$ for this scenario is given by

$$\mathbf{k}_n(m) = \frac{\left(\sqrt{\frac{2}{\pi}}\right)\hat{\mathbf{M}}_{n|n-1}(m,m)}{\sqrt{\mathbf{C}_r(m,m) + \hat{\mathbf{M}}_{n|n-1}(m,m)}}. \quad (55)$$

Finally, the expression for the MSE in (43) can be derived by substituting the expression for $\mathbf{k}_n(m)$ above into (55) and simplifying it as shown below

$$\begin{aligned} \hat{\mathbf{M}}_{n|n}(m,m) &= \mathbb{E}\{\left(\mathbf{x}_n(m) - \hat{\mathbf{x}}_{n|n-1}(m) - \mathbf{k}_n(m)\,\mathbf{v}_n(m)\right)^2\} \\ &= \hat{\mathbf{M}}_{n|n-1}(m,m) + (\mathbf{k}_n(m))^2\,\mathbb{E}\{(\mathbf{v}_n(m))^2\} \\ &\quad - 2\mathbf{k}_n(m)\,\mathbb{E}\{\mathbf{v}_n(m)\,\mathbf{x}_n(m)\}. \end{aligned} \quad (56)$$

Employing the result $Pr\{\mathbf{v}_n(m)|\mathbf{v}_{1:n-1}(m)\} = \frac{1}{2}$ together with the total probability rule, one obtains

$$\begin{aligned} &E[\mathbf{v}_n(m)\,\mathbf{x}_n(m)] \\ &= \frac{1}{2}E[\mathbf{x}_n(m)|\mathbf{v}_n(m) = 1] - \frac{1}{2}E[\mathbf{x}_n(m)|\mathbf{v}_n(m) = -1] \\ &= \frac{1}{2}\left(\hat{\mathbf{x}}_{n|n-1}(m) + \mathbf{k}_n(m)\right) - \frac{1}{2}\left(\hat{\mathbf{x}}_{n|n-1}(m) - \mathbf{k}_n(m)\right) \\ &= \mathbf{k}_n(m). \end{aligned} \quad (57)$$

Substituting $\mathbb{E}\{\mathbf{v}_n(m)\,\mathbf{x}_n(m)\}$ from (57) to (56), together with the fact that $E\left[\mathbf{v}_n(m)^2\right] = 1$, leads to the expression for $\hat{\mathbf{M}}_{n|n}(m,m)$ given below.

$$\hat{\mathbf{M}}_{n|n}(m,m) = \hat{\mathbf{M}}_{n|n-1}(m,m) - (\mathbf{k}_n(m))^2. \quad (58)$$

Finally, substituting the expression for the Kalman gain $\mathbf{k}_n(m)$ from (55) into the above equation yields the variance update rule of (43).

APPENDIX B
SIMPLIFICATION OF ESTIMATION UPDATE EQUATION (54)

To simplify the analysis, the vector and matrix elements are replaced by their respective scalar quantities after dropping the measurement index m. Thus, the various quantities can be expressed as $\hat{x}_{n|n-1} := \hat{\mathbf{x}}_{n|n-1}(m)$, $\hat{M}_{n|n-1} := \hat{\mathbf{M}}_{n|n-1}(m,m)$ and $C_r := \mathbf{C}_r(m,m)$. Considering the case when $\mathbf{v}_n(m) = 1$ and substituting $\tilde{x}_n \triangleq x_n - \hat{x}_{n|n-1}$, equation (51) can be recast as

$$\hat{x}_{n|n} = \hat{x}_{n|n-1} + 2\int_{\mathbb{R}} \tilde{x}_n Q\left[-\frac{\tilde{x}_n}{\sqrt{C_r}}\right] \frac{\exp\left[\frac{-\tilde{x}_n^2}{2\hat{M}_{n|n-1}}\right]}{\sqrt{2\pi\hat{M}_{n|n-1}}} d\tilde{x}_n. \quad (59)$$

Algorithm 5 KF Based Dynamic State Estimation

Input Data: $\mathbf{z}_{1:n}$, $\mathbf{x}_1$, $\mathbf{x}_2$
Input Parameter: $\mathbf{C}_q$, $\mathbf{C}_r$, Holt parameters w_1, w_2
Initialize: $\hat{\mathbf{x}}_{1|1} = \mathbf{x}_1$, $\hat{\mathbf{M}}_{1|1} = \mathbf{C}_q$, $\mathbf{a}_1 = \mathbf{x}_1$, $\mathbf{b}_1 = \mathbf{x}_2 - \mathbf{x}_1$ and $\mathbf{g}_1$ using (7).
Evaluate: $\mathbf{F}_n$ using (6).
for n=2 to N **do**

1. State prediction: $\hat{\mathbf{x}}_{n|n-1} = \mathbf{F}_{n-1}\hat{\mathbf{x}}_{n-1|n-1} + \mathbf{g}_{n-1}$
2. Evaluate innovation $\hat{\mathbf{z}}_{n|n-1}$ as $\tilde{\mathbf{z}}_{n|n-1} = \mathbf{z}_n - \hat{\mathbf{z}}_{n|n-1} = \mathbf{z}_n - \hat{\mathbf{x}}_{n|n-1}$.
3. Update $\mathbf{g}_n$ using (7).
4. Prediction error covariance update

$$\hat{\mathbf{M}}_{n|n-1} = \mathbf{F}_n\hat{\mathbf{M}}_{n-1|n-1}\mathbf{F}_n^T + \mathbf{C}_q$$

5. Evaluate Kalman gain matrix ($P \times M$)

$$\mathbf{K}_n = \hat{\mathbf{M}}_{n|n-1}\left(\mathbf{C}_r + \hat{\mathbf{M}}_{n|n-1}\right)^{-1}$$

6. Correction step

$$\hat{\mathbf{x}}_{n|n} = \hat{\mathbf{x}}_{n|n-1} + \mathbf{K}_n\tilde{\mathbf{z}}_{n|n-1}$$

7. Estimation error covariance update

$$\hat{\mathbf{M}}_{n|n} = (\mathbf{I} - \mathbf{K}_n)\,\hat{\mathbf{M}}_{n|n-1}$$

8. Update $\mathbf{a}_n$ and $\mathbf{b}_n$ using (8) and (9) respectively.

end for

On substituting $\tilde{u}_n = \frac{\tilde{x}_n}{\sqrt{\hat{M}_{n|n-1}}}$, the integral in the above expression reduces to

$$I = \frac{2\sqrt{\hat{M}_{n|n-1}}}{\sqrt{2\pi}}\int_{\mathbb{R}} \tilde{u}_n Q\left[-\tilde{u}_n\frac{\sqrt{\hat{M}_{n|n-1}}}{\sqrt{C_r}}\right]\exp\left[\frac{-\tilde{u}_n^2}{2}\right]d\tilde{u}_n \tag{60}$$

$$I = \frac{2\sqrt{\hat{M}_{n|n-1}}}{\sqrt{2\pi}}\int_{\mathbb{R}} \tilde{u}_n \exp\left[\frac{-\tilde{u}_n^2}{2}\right] \times\left(\frac{1}{\sqrt{2\pi}}\int_{-\tilde{u}_n\frac{\sqrt{\hat{M}_{n|n-1}}}{\sqrt{C_r}}}^{\infty}\exp\left[\frac{-t^2}{2}\right]dt\right)d\tilde{u}_n. \tag{61}$$

Employing $l_1 = \frac{-t\sqrt{C_r}}{\sqrt{\hat{M}_{n|n-1}}}$ and interchanging the integrals above, followed by further simplifications yields,

$$I = \frac{\sqrt{\hat{M}_{n|n-1}}}{\pi}\int_{\mathbb{R}}\exp\left[\frac{-t^2}{2}\right]\int_{l_1}^{\infty}\tilde{u}_n\exp\left[\frac{-\tilde{u}_n^2}{2}\right]d\tilde{u}_n dt \tag{62}$$

$$I = \frac{\sqrt{\hat{M}_{n|n-1}}}{\pi}\int_{\mathbb{R}}\exp\left[\frac{-t^2}{2}\right]\int_{l_1}^{\infty}\left(\frac{-\partial}{\partial\tilde{u}_n}\right)\exp\left[\frac{-\tilde{u}_n^2}{2}\right]d\tilde{u}_n dt \tag{63}$$

$$I = \frac{\sqrt{\hat{M}_{n|n-1}}}{\pi}\int_{\mathbb{R}}\exp\left[\frac{-t^2}{2}\right]\left(-\exp\left[\frac{-\tilde{u}_n^2}{2}\right]\right)\Big|_{(\tilde{u}_n=l_1)}^{(\tilde{u}_n=\infty)}dt \tag{64}$$

$$I = \frac{\sqrt{\hat{M}_{n|n-1}}}{\pi}\int_{\mathbb{R}}\exp\left[\frac{-t^2}{2}\left(1+\frac{C_r}{\hat{M}_{n|n-1}}\right)\right]dt. \tag{65}$$

Hence, the MMSE estimate can be determined as

$$\hat{x}_{n|n} = \hat{x}_{n|n-1} + \frac{\sqrt{\hat{M}_{n|n-1}}}{\pi}\left(\frac{\sqrt{2\pi}}{\sqrt{\left(1+\frac{C_r}{\hat{M}_{n|n-1}}\right)}}\right), \tag{66}$$

$$\hat{x}_{n|n} = \hat{x}_{n|n-1} + \sqrt{\frac{2}{\pi}}\left(\frac{\hat{M}_{n|n-1}}{\sqrt{\hat{M}_{n|n-1}+C_r}}\right). \tag{67}$$

The MMSE estimate for $\mathbf{v}_n(m) = -1$ can also be determined similarly and its expression is given in (55).

APPENDIX C
DYNAMIC STATE ESTIMATION USING KALMAN FILTER

The Kalman filter for dynamic estimation of the state sequence $\hat{\mathbf{x}}_n$ with analog error-free transmission of the measurements $\mathbf{z}_n$, for the state evolution model given in (5) and linear measurement model in (2), is briefly summarized in Algorithm 5.

ACKNOWLEDGMENT

The authors would like to thank Sreenath J. G., Department of Electrical Engineering, IIT Kanpur, Kanpur, UP, India and Rahul R. Jha, School of Electrical Engineering and Computer Science, Washington State University, Pullman, WA, USA, for their valuable comments and suggestions. The authors are also grateful for support from the TCS research scholarship program at IIT Kanpur.

REFERENCES

[1] S. M. Amin and B. F. Wollenberg, "Toward a smart grid: Power delivery for the 21st century," *IEEE Power Energy Mag.*, vol. 3, no. 5, pp. 34–41, Sep./Oct. 2005.
[2] M. H. Rehmani, M. E. Kantarci, A. Rachedi, M. Radenkovic, and M. Reisslein, "IEEE access special section editorial smart grids: A hub of interdisciplinary research," *IEEE Access*, vol. 3, pp. 3114–3118, 2015.
[3] X. Fang, S. Misra, G. Xue, and D. Yang, "Smart grid—The new and improved power grid: A survey," *IEEE Commun. Surveys Tuts.*, vol. 14, no. 4, pp. 944–980, 4th Quart., 2012.
[4] H. Farhangi, "The path of the smart grid," *IEEE Power Energy Mag.*, vol. 8, no. 1, pp. 18–28, Jan. 2010.
[5] H. A. H. Hassan, A. Pelov, and L. Nuaymi, "Integrating cellular networks, smart grid, and renewable energy: Analysis, architecture, and challenges," *IEEE Access*, vol. 3, pp. 2755–2770, 2015.
[6] A. Ahmed *et al.*, "Multiple power line outage detection in smart grids: Probabilistic Bayesian approach," *IEEE Access*, vol. 6, pp. 10650–10661, 2018.
[7] J. D. Kueck, R. H. Staunton, S. D. Labinov, and B. J. Kirby, "Microgrid energy management system," Oak Ridge Nat. Lab., Oak Ridge, TN, USA, Tech. Rep. ORNL/TM-2002/242, Jan. 2003.
[8] D. Niyato, L. Xiao, and P. Wang, "Machine-to-machine communications for home energy management system in smart grid," *IEEE Commun. Mag.*, vol. 49, no. 4, pp. 53–59, Apr. 2011.
[9] A. Abur and A. G. Exposito, *Power System State Estimation: Theory Implement*. Boca Raton, FL, USA: CRC Press, 2004.

[10] Y.-F. Huang, S. Werner, J. Huang, N. Kashyap, and V. Gupta, "State estimation in electric power grids: Meeting new challenges presented by the requirements of the future grid," *IEEE Signal Process. Mag.*, vol. 29, no. 5, pp. 33–43, Sep. 2012.

[11] R. Ma, H.-H. Chen, Y.-R. Huang, and W. Meng, "Smart grid communication: Its challenges and opportunities," *IEEE Trans. Smart Grid*, vol. 4, no. 1, pp. 36–46, Mar. 2013.

[12] P. P. Parikh, M. G. Kanabar, and T. S. Sidhu, "Opportunities and challenges of wireless communication technologies for smart grid applications," in *Proc. IEEE PES General Meeting*, Jul. 2010, pp. 1–7.

[13] D. Baimel, S. Tapuchi, and N. Baimel, "Smart grid communication technologies- overview, research challenges and opportunities," in *Proc. Int. Symp. Power Electron., Electr. Drives, Autom. Motion (SPEEDAM)*, Jun. 2016, pp. 116–120.

[14] V. C. Gungor *et al.*, "Smart grid technologies: Communication technologies and standards," *IEEE Trans. Ind. Informat.*, vol. 7, no. 4, pp. 529–539, Nov. 2011.

[15] Y. Yan, Y. Qian, H. Sharif, and D. Tipper, "A survey on smart grid communication infrastructures: Motivations, requirements and challenges," *IEEE Commun. Surveys Tuts.*, vol. 15, no. 1, pp. 5–20, Feb. 2013.

[16] C. Kalalas, L. Thrybom, and J. Alonso-Zarate, "Cellular communications for smart grid neighborhood area networks: A survey," *IEEE Access*, vol. 4, pp. 1469–1493, 2016.

[17] V. C. Gungor *et al.*, "A survey on smart grid potential applications and communication requirements," *IEEE Trans. Ind. Informat.*, vol. 9, no. 1, pp. 28–42, Feb. 2013.

[18] M. M. Rana, L. Li, and S. Su, "Distributed state estimation using RSC coded smart grid communications," *IEEE Access*, vol. 3, pp. 1340–1349, 2015.

[19] N. Pavlidou, A. J. H. Vinck, J. Yazdani, and B. Honary, "Power line communications: State of the art and future trends," *IEEE Commun. Mag.*, vol. 41, no. 4, pp. 34–40, Apr. 2003.

[20] D. Tse and P. Viswanath, *Fundamentals Wireless Communication*. Cambridge, U.K.: Cambridge Univ. Press, 2005.

[21] P. S. Maruvada, *Corona Performs High-Voltage Transmiss. Lines*. Baldock, U.K.: Research Studies Press, 2000.

[22] J. I. Huertas, R. Barraza, and J. M. Echeverry, "Wireless data transmission from inside electromagnetic fields," in *Proc. 6th Int. Conf. Electr. Eng., Comput. Sci. Autom. Control*, Jan. 2009, pp. 1–7.

[23] J. N. Laneman, E. Martinian, G. W. Wornell, and J. G. Apostolopoulos, "Source-channel diversity for parallel channels," *IEEE Trans. Inf. Theory*, vol. 51, no. 10, pp. 3518–3539, Oct. 2005.

[24] V. K. Goyal, "Multiple description coding: Compression meets the network," *IEEE Signal Process. Mag.*, vol. 18, no. 5, pp. 74–93, Sep. 2001.

[25] A. Sharma and S. R. Samantaray, "Power system tracking state estimator for smart grid under unreliable PMU data communication network," *IEEE Sensors J.*, vol. 18, no. 5, pp. 2107–2116, Mar. 2018.

[26] L. I. Rudin, S. Osher, and E. Fatemi, "Nonlinear total variation based noise removal algorithms," *Phys. D, Nonlinear Phenomena*, vol. 60, nos. 1–4, pp. 259–268, 1992.

[27] S. H. Chan, R. Khoshabeh, K. B. Gibson, P. E. Gill, and T. Q. Nguyen, "An augmented Lagrangian method for total variation video restoration," *IEEE Trans. Image Process.*, vol. 20, no. 11, pp. 3097–3111, Nov. 2011.

[28] A. Kudeshia and A. K. Jagannatham, "Optimal Viterbi based total variation sequence detection (TVSD) for robust image/video decoding in wireless sensor Networks," *IEEE Signal Process. Lett.*, vol. 21, no. 6, pp. 722–726, Jun. 2014.

[29] C. Li, "An efficient algorithm for total variation regularization with applications to the single pixel camera and compressive sensing," M.S. thesis, Dept. Comput. Appl. Math., Rice Univ., Houston, TX, USA, Sep. 2009.

[30] A. S. Debs and R. E. Larson, "A dynamic estimator for tracking the state of a power system," *IEEE Trans. Power App. Syst.*, vol. PAS-89, no. 7, pp. 1670–1678, Sep. 1970.

[31] K. Nishiya, J. Hasegawa, and T. Koike, "Dynamic state estimation including anomaly detection and identification for power systems," *IEE Proc. C—Gener., Transmiss. Distrib.*, vol. 129, no. 5, pp. 192–198, Sep. 1982.

[32] A. M. L. D. Silva, M. B. D. C. Filho, and J. M. C. Cantera, "An efficient dynamic state estimation algorithm including bad data processing," *IEEE Trans. Power Syst.*, vol. 2, no. 4, pp. 1050–1058, Nov. 1987.

[33] G. Durgaprasad and S. S. Thakur, "Robust dynamic state estimation of power systems based on M-estimation and realistic modeling of system dynamics," *IEEE Trans. Power Syst.*, vol. 13, no. 4, pp. 1331–1336, Nov. 1998.

[34] N. Shivakumar and A. Jain, "A review of power system dynamic state estimation techniques," in *Proc. Joint Int. Conf. Power Syst. Technol. IEEE Power India Conf.*, Oct. 2008, pp. 1–6.

[35] R. Dhaouadi, N. Mohan, and L. Norum, "Design and implementation of an extended Kalman filter for the state estimation of a permanent magnet synchronous motor," *IEEE Trans. Power Electron.*, vol. 6, no. 3, pp. 491–497, Jul. 1991.

[36] G. Valverde and V. Terzija, "Unscented Kalman filter for power system dynamic state estimation," *IET Generat., Transmiss. Distrib.*, vol. 5, no. 1, pp. 29–37, Jan. 2011.

[37] S. Haykin, *Communication Systems*. Hoboken, NJ, USA: Wiley, 2008.

[38] S. M. Kay, *Fundamentals of Statistical Signal Processing, Volume I: Estimation Theory*. Upper Saddle River, NJ, USA: Prentice-Hall, 1993.

[39] G. Krumpholz, K. Clements, and P. Davis, "Power system observability: A practical algorithm using Network topology," *IEEE Trans. Power App. Syst.*, vol. PAS-99, no. 4, pp. 1534–1542, Jul. 1980.

[40] S. Chakrabarti and E. Kyriakides, "Optimal placement of phasor measurement units for power system observability," *IEEE Trans. Power Syst.*, vol. 23, no. 3, pp. 1433–1440, Aug. 2008.

[41] A. Phadke, J. S. Thorp, R. F. Nuqui, and M. Zhou, "Recent developments in state estimation with phasor measurements," in *Proc. IEEE Power Syst. Conf. Exposit.*, Mar. 2009, pp. 1–7.

[42] A. Leite da Silva, M. B. Do Coutto Filho, and J. F. de Queiroz, "State forecasting in electric power systems," *IEE Proc. C—Generat., Transmiss. Distrib.*, vol. 130, no. 5, pp. 237–244, 1983.

[43] F. F. Wu, "Power system state estimation: A survey," *Int. J. Elect. Power Energy Syst.*, vol. 12, no. 2, pp. 80–87, 1990.

[44] V. Kekatos and G. B. Giannakis, "Distributed robust power system state estimation," *IEEE Trans. Power Syst.*, vol. 28, no. 2, pp. 1617–1626, May 2013.

[45] F. C. Schweppe and J. Wildes, "Power system static-state estimation, Part I: Exact model," *IEEE Trans. Power App. Syst.*, vol. PAS-89, no. 1, pp. 120–125, Jan. 1970.

[46] F. C. Schweppe and D. B. Rom, "Power system static-state estimation, Part II: Approximate model," *IEEE Trans. Power App. Syst.*, vol. PAS-89, no. 1, pp. 125–130, Jan. 1970.

[47] F. Schweppe, "Power system static-state estimation, part III: Implementation," *IEEE Trans. Power App. Syst.*, vol. PAS-89, no. 1, pp. 130–135, Jan. 1970.

[48] P. Rousseaux, T. van Cutsem, and T. D. Liacco, "Whither dynamic state estimation?" *Int. J. Electr. Power Energy Syst.*, vol. 12, no. 2, pp. 104–116, Apr. 1990.

[49] A. Mahalanabis, K. Biswas, and G. Singh, "An algorithm for decoupled dynamic state estimators of power systems," in *Proc. IEEE PES Summer Meeting*. Los Angeles, CA, USA, Jul. 1978, pp. 573–578.

[50] J.-C. Guey, M. P. Fitz, M. R. Bell, and W.-Y. Kuo, "Signal design for transmitter diversity wireless communication systems over Rayleigh fading channels," *IEEE Trans. Commun.*, vol. 47, no. 4, pp. 527–537, Apr. 1999.

[51] B. Sklar, "Rayleigh fading channels in mobile digital communication systems. I. Characterization," *IEEE Commun. Mag.*, vol. 35, no. 7, pp. 90–100, Jul. 1997.

[52] G. J. Foschini and M. J. Gans, "On limits of wireless communications in a fading environment when using multiple antennas," *Wireless Pers. Commun.*, vol. 6, no. 3, pp. 311–335, Mar. 1998.

[53] L. Lu, G. Y. Li, A. L. Swindlehurst, A. Ashikhmin, and R. Zhang, "An overview of massive MIMO: Benefits and challenges," *IEEE J. Sel. Topics Signal Process.*, vol. 8, no. 5, pp. 742–758, Oct. 2014.

[54] D. Strong and T. Chan, "Edge-preserving and scale-dependent properties of total variation regularization," *Inverse Problems*, vol. 19, no. 6, p. S165, Nov. 2003.

[55] R. Acar and C. R. Vogel, "Analysis of bounded variation penalty methods for ill-posed problems," *Inverse Problems*, vol. 10, no. 6, p. 1217, 1994.

[56] K. Kunisch and M. Hintermüller, "Total bounded variation regularization as a bilaterally constrained optimization problem," *SIAM J. Appl. Math.*, vol. 64, no. 4, pp. 1311–1333, 2004.

[57] V. Y. Panin, G. L. Zeng, and G. T. Gullberg, "Total variation regulated EM algorithm [SPECT reconstruction]," *IEEE Trans. Nucl. Sci.*, vol. 46, no. 6, pp. 2202–2210, Dec. 1999.

[58] A. Monticelli, "Electric power system state estimation," *Proc. IEEE*, vol. 88, no. 2, pp. 262–282, Feb. 2000.

[59] C.-W. Shu, "Total-variation-diminishing time discretizations," *SIAM J. Sci. Statist. Comput.*, vol. 9, no. 6, pp. 1073–1084, 1988.

[60] D. L. Donoho, "Compressed sensing," *IEEE Trans. Inf. Theory*, vol. 52, no. 4, pp. 1289–1306, Apr. 2006.
[61] P. Kansal and A. Bose, "Bandwidth and latency requirements for smart transmission grid applications," *IEEE Trans. Smart Grid*, vol. 3, no. 3, pp. 1344–1352, Sep. 2012.
[62] R. Steele, "SNR formula for linear delta modulation with band-limited flat and RC-shaped Gaussian signals," *IEEE Trans. Commun.*, vol. 28, no. 12, pp. 1977–1984, 1980.
[63] R. Steele, *Delta Modulation Systems*. London, U.K.: Pentech Press, 1975.
[64] K. K. Mukkavilli, A. Sabharwal, E. Erkip, and B. Aazhang, "On beamforming with finite rate feedback in multiple-antenna systems," *IEEE Trans. Inf. Theory*, vol. 49, no. 10, pp. 2562–2579, Oct. 2003.
[65] J. Sanchez-Garcia, L. Soriano-Equigua, and R. W. Heath, Jr., "Quantized antenna combining for multiuser MIMO-OFDM with limited feedback," *IEEE Signal Process. Lett.*, vol. 16, no. 12, pp. 1027–1030, Dec. 2009.
[66] D. J. Love and R. W. Heath, "Limited feedback diversity techniques for correlated channels," *IEEE Trans. Veh. Technol.*, vol. 55, no. 2, pp. 718–722, Mar. 2006.
[67] A. D. Dabbagh and D. J. Love, "Feedback rate-capacity loss tradeoff for limited feedback MIMO systems," *IEEE Trans. Inf. Theory*, vol. 52, no. 5, pp. 2190–2202, May 2006.
[68] D. J. Love, R. W. Heath, and T. Strohmer, "Grassmannian beamforming for multiple-input multiple-output wireless systems," in *Proc. IEEE Int. Conf. Commun.*, Oct. 2003, pp. 2618–2622.
[69] T. Inoue and R. W. Heath, "Grassmannian predictive coding for limited feedback multiuser MIMO systems," in *Proc. IEEE Int. Conf. Acoust., Speech Signal Process. (ICASSP)*, May 2011, pp. 3076–3079.
[70] J. Zhang, L. Dai, X. Li, Y. Liu, and L. Hanzo, "On low-resolution ADCs in practical 5G millimeter-wave massive MIMO systems," *IEEE Commun. Mag.*, vol. 56, no. 7, pp. 205–211, Jul. 2018.
[71] A. Ribeiro, G. B. Giannakis, and S. I. Roumeliotis, "SOI-KF: Distributed Kalman filtering with low-cost communications using the sign of innovations," *IEEE Trans. Signal Process.*, vol. 54, no. 12, pp. 4782–4795, Dec. 2006.
[72] (2016). *Power Systems Test Case Archive*. [Online]. Available: https://www2.ee.washington.edu/research/pstca
[73] Q. Zhang, Y. Chakhchoukh, V. Vittal, G. T. Heydt, N. Logic, and S. Sturgill, "Impact of PMU measurement buffer length on state estimation and its optimization," *IEEE Trans. Power Syst.*, vol. 28, no. 2, pp. 1657–1665, May 2013.
[74] A. Sharma, S. C. Srivastava, and S. Chakrabarti, "A cubature Kalman filter based power system dynamic state estimator," *IEEE Trans. Instrum. Meas.*, vol. 66, no. 8, pp. 2036–2045, Aug. 2017.
[75] K. Das, J. Hazra, D. P. Seetharam, R. K. Reddi, and A. K. Sinha, "Real-time hybrid state estimation incorporating SCADA and PMU measurements," in *Proc. 3rd IEEE PES Innov. Smart Grid Technol. Eur.*, Oct. 2012, pp. 1–8.
[76] (2017). *G.B. National Grid Status*. [Online]. Available: http://www.gridwatch.templar.co.uk
[77] E. Sulaiman, M. Saufi, M. Zarafi, and B. Kok, "Laboratory testing on overhead line for various load conditions," in *Proc. IEEE 2nd Int. Power Energy Conf. (PECon)*, Dec. 2008, pp. 1677–1681.
[78] A. K. Al-Othman and M. R. Irving, "Uncertainty modelling in power system state estimation," *IET Generat., Transmiss. Distrib.*, vol. 152, no. 2, pp. 233–239, Mar. 2005.
[79] S. Chakrabarti, E. Kyriakides, G. Ledwich, and A. Ghosh, "Inclusion of PMU current phasor measurements in a power system state estimator," *IET Generat., Transmiss. Distrib.*, vol. 4, no. 10, pp. 1104–1115, Oct. 2010.
[80] J. Zhao, G. Zhang, and M. L. Scala, "A two-stage robust power system state estimation method with unknown measurement noise," in *Proc. IEEE Power Energy Society General Meeting (PESGM)*, Jul. 2016, pp. 1–5.
[81] C.-L. Su and C.-N. Lu, "Interconnected network state estimation using randomly delayed measurements," *IEEE Trans. Power Syst.*, vol. 16, no. 4, pp. 870–878, Nov. 2001.
[82] C. K. Wen, C. J. Wang, S. Jin, K. K. Wong, and P. Ting, "Bayes-optimal joint channel-and-data estimation for massive MIMO with low-precision ADCs," *IEEE Trans. Signal Process.*, vol. 64, no. 10, pp. 2541–2556, May 2016.
[83] J. Mo and R. W. Heath, Jr., "Capacity analysis of one-bit quantized MIMO systems with transmitter channel state information," *IEEE Trans. Signal Process.*, vol. 63, no. 20, pp. 5498–5512, Oct. 2015.

ANKIT KUDESHIA (S'13) received the B.Tech. degree in electronics and communication engineering from the Indian Institute of Information Technology, Design and Manufacturing, Jabalpur, India, in 2010. He is currently pursuing the M.Tech. and Ph.D. dual degrees with the Department of Electrical Engineering, IIT Kanpur, India. His research interests include signal processing techniques for wireless communications, smart grids, and wireless multimedia sensor networks. He received the Prestigious TCS-RSP Fellowship for pursuing Ph.D. studies in computing sciences at IIT Kanpur from 2014 to 2018.

ADITYA K. JAGANNATHAM (M'05) received the bachelor's degree from the IIT Bombay, Mumbai, and the M.S. and Ph.D. degrees from the University of California at San Diego, San Diego, USA. From 2007 to 2009, he was a Senior Wireless Systems Engineer with Qualcomm, Inc., San Diego, CA, USA, where he worked on developing 3G UMTS/WCDMA/HSDPA mobile chipsets as part of the Qualcomm CDMA Technologies Division. Since 2009, he has been a Faculty Member with the Electrical Engineering Department, IIT Kanpur, where he is currently an Associate Professor, and is also associated with the BSNL-IITK Telecom Center of Excellence. His research interests include next-generation wireless communications and networking, sensor and ad-hoc networks, digital video processing for wireless systems, wireless 3G/4G cellular standards, and CDMA/OFDM/MIMO wireless technologies. He has contributed to the 802.11n high throughput wireless LAN standard. He received the CAL(IT)2 Fellowship for pursuing graduate studies at the University of California at San Diego and, in 2009, he received the Upendra Patel Achievement Award for his efforts towards developing HSDPA/HSUPA/HSPA+WCDMA technologies at Qualcomm. At IIT Kanpur, he received the P.K. Kelkar Young Faculty Research Fellowship from 2012 to 2015 for excellence in research and the Gopal Das Bhandari Memorial Distinguished Teacher Award for the year 2012–2013 for excellence in teaching. He has also delivered a set of video lectures on Advanced 3G and 4G Wireless Mobile Communications for the Ministry of Human Resource Development funded initiative National Programme on Technology Enhanced Learning.

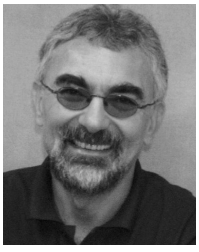

LAJOS HANZO (F'04) received the degree in electronics in 1976 and the Ph.D. degree in 1983. He is currently pursuing the D.Sc. degree. In 2009, he received an honorary doctorate by the Technical University of Budapest and in 2015 by The University of Edinburgh. In 2016, he was admitted to the Hungarian Academy of Science. During his 40-year career in telecommunications, he has held various research and academic posts in Hungary, Germany, and U.K. Since 1986, he has been with the School of Electronics and Computer Science, University of Southampton, U.K., where he holds the Chair in telecommunications. He has successfully supervised 111 Ph.D. students, co-authored 18 John Wiley/IEEE Press books on mobile radio communications totaling in excess of 10000 pages, published 1798 research contributions at IEEE Xplore, acted both as a TPC and a General Chair of IEEE conferences, presented keynote lectures and has been awarded a number of distinctions. He has about 40000 citations. He is a Fellow of Royal Academy of Engineering, IET, and EURASIP. He is currently directing an academic research team, working on a range of research projects in wireless multimedia communications sponsored by industry, the Engineering and Physical Sciences Research Council, U.K., the European Research Council's Advanced Fellow Grant, and the Royal Society's Wolfson Research Merit Award. He is an Enthusiastic Supporter of industrial and academic liaison and he offers a range of industrial courses. He is also a Governor of the IEEE ComSoc and VTS. From 2008 to 2012, he was the Editor-in-Chief of the IEEE Press and a Chaired Professor at Tsinghua University, Beijing.